Spontaneous fusion of MSC with breast cancer cells can generate tumor dormancy

Catharina Melzer
Biochemistry and Tumor Biology Lab, Dept. of Gynecology, Hannover Medical School
Juliane von der Ohe
Biochemistry and Tumor Biology Lab, Dept. of Gynecology, Hannover Medical School
Tianjiao Luo
Biochemistry and Tumor Biology Lab, Dept. of Gynecology, Hannover Medical School
Ralf Hass (hass.ralf@mh-hannover.de)
Hannover Medical School https://orcid.org/0000-0002-2481-7547

Research Article

Keywords: mesenchymal stroma-/stem-like cells, cancer cell fusion, tumor microenvironment, cell interaction

Posted Date: March 22nd, 2021

DOI: https://doi.org/10.21203/rs.3.rs-321562/v1

Spontaneous fusion of MSC with breast cancer cells can generate tumor dormancy

Catharina Melzer [1], Juliane von der Ohe [1], Tianjiao Luo [1], and Ralf Hass [1*]

[1] Biochemistry and Tumor Biology Lab, Department of Obstetrics and Gynecology, Hannover Medical School, 30625 Hannover, Germany;

catharina.melzer@t-online.de (C.M.); Ohe.Juliane.von.der@mh-hannover.de (J.v.d.O.); luo_tj@yeah.net (T.L.);

* Correspondence: hass.ralf@mh-hannover.de; Tel.: +49-511-532-6070

Abstract

Background: A variety of different tumors including breast cancer cells can closely interact with mesenchymal stroma/stem-like cells (MSC) in the tumor microenvironment eventually resulting in cell fusion and formation of new hybrid cancer cell populations displaying altered properties.

Methods: Lentiviral-transduced MDA-MB-231^{cherry} breast cancer cells and MSC^{GFP} were co-cultured and a resulting hybrid cancer cell population (MDA-MSC-hyb5) was isolated. Characterization was performed for marker expression and short tandem repeat (STR) fragment analysis compared to the parental cells. Moreover, in vivo tumor development and metastatic capacity of MDA-MSC-hyb5 was studied and unique properties were analyzed by RNA microarray expression analyses compared to other breast cancer hybrid populations. Potential chemotherapeutic sensitivity was carried out in tumor explant cultures of MDA-MSC-hyb5 cells.

Results: Direct cellular interactions of MDA-MB-231^{cherry} breast cancer cells with MSC^{GFP} in a co-culture model resulted in spontaneous cell fusion by generation of MDA-MSC-hyb5$^{cherry\ GFP}$ breast cancer hybrid cells. Proliferative capacity of MDA-MSC-hyb5 cells was about 1.8-fold enhanced when compared to the parental MDA-MB-231^{cherry} breast cancer cells. In contrast to a

spontaneous MDA-MB-231^{cherry}-induced tumor development in vivo within 18.8 days MDA-MSC-hyb5 cells initially remained quiescent in a dormancy-like state. At distinct time points up to about a half year later after injection NODscid mice started to develop MDA-MSC-hyb5 cell-induced tumors. Following tumor initiation, formation of metastases in various different organs occurred rapidly within about 10.5 days. Changes in gene expression levels were evaluated by RNA-microarray analysis and revealed certain increase in dormancy-associated transcripts in MDA-MSC-hyb5. Chemotherapeutic responsiveness of MDA-MSC-hyb5 cells was partially enhanced as compared to MDA-MB-231 cells, however, some resistance e.g. for taxol was detectable in cancer hybrid cells. Moreover, drug response partially changed during tumor development of MDA-MSC-hyb5 cells suggesting unstable in vivo phenotypes of MDA-hyb5 cells with increased tumor heterogeneity.

Conclusions: The spontaneous formation of cancer hybrid cell populations like MDA-MSC-hyb5 by cell fusion contributes to tumorigenic diversification by acquisition of new properties such as altered chemotherapeutic responsiveness. The unique tumor dormancy of MDA-MSC-hyb5 cells not observed in other breast cancer hybrid cells so far markedly increases tumor heterogeneity.

Plain English summary

Cell fusion as a fundamental biological process is required for various physiological processes, including fertilization, placentation, myogenesis, osteoclastogenesis, and wound healing/tissue regeneration. However, cell fusion is also observed during pathophysiological processes like tumor development. Mesenchymal stroma/stem-like cells (MSC) which play an important role within the tumor microenvironment can closely interact and eventually fuse e.g. with breast cancer cells. During this rare event the resulting breast cancer/MSC hybrid cells undergo a post-hybrid selection process (PHSP) to reorganize chromosomes of the two parental nuclei whereby the majority of the hybrid population undergoes cell death. Although the PHSP-surviving hybrid cancer cells represent an initially small minority within the tumor tissue, their changed properties may provide

a proliferation advantage eventually overgrowing other cancer cells. These properties were observed after spontaneous fusion of MDA-MB-231 breast cancer cells with human MSC forming the new MDA-MSC-hyb5 cells. Displaying an altered DNA profile compared to the parental cells, MDA-MSC-hyb5 cells demonstrated initial tumor dormancy when transplanted into NODscid mice. After a lag period of up to 6 months, however, MDA-MSC-hyb5 cells suddenly initiated tumor growth and metastatic spreading much more enhanced compared to the parental MDA-MB-231 cells. This initial tumor dormancy not observed in other breast cancer hybrid populations was associated with a corresponding gene expression profile. Accordingly, chemotherapeutic responsiveness was significantly altered in MDA-MSC-hyb5 cells. These unique properties of MDA-MSC-hyb5 cells compared to other breast cancer hybrid cells provide a platform to further study diversification and elevated tumor plasticity together with molecular traits of tumor dormancy.

Keywords: mesenchymal stroma-/stem-like cells; cancer cell fusion; tumor microenvironment; cell interaction;

Background

Cell fusion in general is considered a rare event although its actual frequency may be higher as postulated by "hidden" fusions [1]. Physiological processes of cell fusion among others include myoblast fusion to form multinucleated myocytes in muscle fibers during muscle development, fusion of mononuclear precursor cells contributing to osteoclast formation for the maintenance, repair, and remodelling of bone tissue, or fusion of fetal trophoblasts to syncytiotrophoblasts during formation of placenta tissue and barrier [2, 3]. Alternatively, cell fusion can occur during pathophysiological processes such as cancer development. Indeed, cell fusion can be detected in various different cancers including leukocyte-tumor cell fusions or macrophage-tumor cell fusions

e.g. brain metastases of melanoma, lung cancer, gastric cancer or different tumors of the breast [3-9]. Breast cancer cell fusion and subsequent generation of breast cancer hybrid/chimeric cells is observed during close interaction of cancer cells with adjacent cell types in the tumor microenvironment like mesenchymal stroma/stem-like cells (MSC) [10-12].

Predominant locations of MSC are perivascular regions of various adult organs and tissues [13, 14]. In addition, neonatal tissues like human umbilical cord (hUC) provide non-invasive MSC-rich sources with superior growth and expansion capacity [15]. Due to their different tissue origin and altered properties MSC display a heterogeneous population also termed multipotent stromal cells or medicinal signaling cells [16, 17]. For in vitro functions, MSC exhibit adherence, migratory activity, differentiation capacity at least along mesenchymal phenotypes, and distinct core surface marker expression like CD73, CD90, and CD105 with simultaneous absence of at least CD14, CD31, CD34, and CD45. While these properties represent minimal characteristics of MSC as stromal cells further specific markers or stem-like capabilities such as self-renewal capacity may only apply to a small subset within a MSC population. Accordingly, MSC heterogeneity is comprised by various subpopulations of stromal cells, stem-like cells and cells with further special properties all displaying the minimal MSC characteristics which can be maintained during prolonged in vitro culture [18] or in a permanently proliferating human MSC-like model with reproducible properties [19]. Moreover, these minimal characteristics are also shared by more differentiated populations such as pericytes and fibroblasts. However, the properties of MSC can change in an altered environment with diverse stimuli in vitro and in vivo [20, 21] which also depends on interacting cell types. In this context, MSC predominantly interact with cancer cells within the tumor microenvironment by various indirect and direct communication mechanisms [22, 23]. Strong interactions which co-localize the two adjacent cell membranes of MSC and cancer cells in close proximity and reorganize actin-associated cytoskeletal proteins can eventually result in the generation of corresponding hybrid/chimeric cancer cells [24, 25].

Various tumor fusions including breast cancer cell fusions with MSC are described [10, 26-29] whereby the resulting breast cancer hybrid cells can display altered tumorigenic activities when compared to the parental cancer cells. Within the tumor microenvironment cancer cells can also fuse with other cell types such as endothelial cells [30]. Although precise mechanisms appear diverse among different cancer cell fusions previous work demonstrated TNF-related signaling and apoptosis as potential triggers for breast cancer fusion with MSC [10, 12, 31].

MSC/breast cancer cell fusion can also occur in vivo whereby associated processes including apoptosis and reorganization of the actin cytoskeleton contribute to an elevated tumor plasticity and heterogeneity with a likely generation of breast cancer stem cells [24, 29, 32, 33]. Likewise, fusion of bone marrow-derived MSC with lung cancer cells generate new cancer hybrid cell population displaying altered properties including cancer stem cell-like properties [34]. Moreover, hybrids from neoplastic but also from normal breast epithelial cells can display stem-like characteristics [35].

Cancer cell fusion generates chromosomal instability and aneuploidy by hybrid cell formation, whereby different polyploid cancer hybrid populations arise and increase tumor heterogeneity. Moreover, new properties of breast cancer hybrid cells also contribute to enhanced metastases [11, 26, 27]. The relevance of fusion processes for the generation of new cancer cell populations is underscored by the findings that MSC/breast cancer cell fusion can generate various different hybrid subtypes (e.g. MDA-MSC-hyb1 to MDA-MSC-hyb4 briefly termed MDA-hyb1 to MDA-hyb4). These cells display different tumorigenic potential, altered metastatic behavior, and changes in their sensitivity to chemotherapeutic drugs which elevates tumor heterogeneity and the potential of breast cancer stem cell expansion. In particular, human MDA-hyb1 and to a lesser extend MDA-hyb2 cancer hybrid cells represent aggressive and highly metastatic breast cancer cell lines originated after spontaneous cell fusion of primary hUC-MSC with the MDA-MB-231 breast cancer cell line. Both, MDA-hyb1 and MDA-hyb2 developed primary tumors and metastases more rapidly as compared to the parental breast cancer cells [11]. Conversely, MDA-hyb3 and MDA-hyb4 breast cancer hybrid cells were isolated following spontaneous fusion with other hUC-MSC primary

cultures and these cancer hybrid populations displayed a reduced tumorigenicity as compared to the parental MDA-MB-231 cells by a markedly prolonged development of primary tumors and distant organ metastases [32].

In the present work, another breast cancer hybrid cell line is created and characterized demonstrating a completely different tumorigenic behavior when compared to the other cancer hybrid populations so far. In contrast to an accelerated tumorigenicity of MDA-hyb1 and MDA-hyb2 and also in contrast to a retarded tumorigenicity of MDA-hyb3 and MDA-hyb4 these new cancer hybrid cells exhibited a third type of tumor behavior by remaining initially dormant and then developing tumors and metastases much faster than the parental breast cancer cells.

Materials and Methods

4.1. Cell Culture

Human MDA-MB-231 breast cancer cells were obtained from the ATCC (#HTB-26) and cultivated initially at 1,500 cells/cm² in Leibovitz's L-15-medium (Invitrogen Life Technologies, Carlsbad, CA, USA) supplemented with 10% (v/v) fetal bovine serum, 100 U/mL penicillin, 100 µg/mL streptomycin and 2 mM L-glutamine (Sigma Chemie GmbH, Taufkirchen, Germany). Subculture of MDA-MB-231 cells was performed by trypsin/EDTA (Biochrom GmbH, Berlin, Germany) treatment for 5 min at 37 °C.

Primary hUC-MSC030816 were isolated from umbilical cord tissue explant cultures as described previously for other MSC [36]. Briefly, hUC-MSC were cultured in MSC growth medium (αMEM (Sigma Chemie GmbH, Steinheim, Germany) supplemented with 10% allogeneic human AB-serum, 100 U/mL penicillin, 100 µg/mL streptomycin and 2 mM L-glutamine (Sigma Chemie GmbH, Taufkirchen, Germany)) and subculture in passages (P) was performed following treatment with accutase (Capricorn Scientific GmbH, Ebsdorfergrund, Germany) at 37°C for 3 min.

All MDA hybrid cell lines (MDA-hyb1 to MDA-hyb5) were cultured at xeno-free conditions in MSC growth medium (αMEM (Sigma Chemie GmbH) supplemented with 10% allogeneic human

AB-serum (blood from male AB donors was commercially obtained from blood bank at Hannover Medical School, Germany, and processed to serum), 100 U/mL penicillin, 100 µg/mL streptomycin and 2 mM L-glutamine (Sigma Chemie GmbH). Subculture in passages (P) was performed following mechanical detachment of the loosely adherent MDA-hyb1 cells and by TrypLE (Life Technologies GmbH, Darmstadt, Germany) treatment of MDA-hyb2, -hyb3, -hyb4, and –hyb5 cells at 37°C for 3 min, respectively.

All cell lines were tested for mycoplasma by the luminometric MycoAlert Plus mycoplasma detection kit (Lonza Inc., Rockland, ME, USA) according to the manufacturer's recommendations. Authentication of the different cell lines was performed by short tandem repeat (STR) fragment analysis using the GenomeLab human STR primer set (Beckman Coulter Inc., Fullerton, CA, USA) [37]. Identity of STR fragments was confirmed for MDA-MB-231 cells according to the STR database provided by the ATCC, Manassas, VA, USA, and for MDA-hyb1 and MDA-hyb2 cell lines as outlined in previous work [11]. For stable fluorescence labeling hUC-MSC and MDA-MB-231 cells were transduced with a 3rd generation lentiviral SIN vector containing the eGFP or the mcherry gene, respectively, as reported elsewhere [38].

4.2. In vitro proliferation and cytotoxicity measurements

The proliferation rate was determined by fluorescence measurement using the fluoroscan assay as previously described [12]. Briefly, 1000 cells/well of MDA-MB-231^{cherry}, MDA-hyb1, MDA-hyb3, or MDA-hyb5 populations were plated in flat bottom 96-well plates (Nunc/ThermoFischer Scientific, Roskilde, Denmark) with (200 µL/well) standard culture medium. MDA-MB-231^{cherry} versus MDA-MB-231^{GFP} demonstrated no differences in proliferative capacity.

For cytotoxicity measurements with different chemotherapeutic agents 1000 cells/well of MDA-MB-231 cells, MDA-hyb5 cells or explant culture cells from MDA-hyb5-derived mouse tumors were plated in flat bottom 96-well plates (Nunc/ThermoFischer Scientific) with (100 µL/well) standard culture medium. The explant culture cells from MDA-hyb5-derived mouse tumors were

obtained by an isolation procedure as extensively described elsewhere for primary human breast cancer epithelial cells [39]. Isolated explant culture cells were subcultured with TrypLE (Life Technologies GmbH) and used in P2 for cytotoxicity measurements. Following overnight attachment of the different cultures 100 µL of drug solvent in culture medium was added as a control, and in further wells 100 µL of culture medium containing appropriate dilutions of epirubicin, taxol, carboplatin, or cyclophosphamide were respectively added to the cells.

After incubation for up to 72 h at the appropriate time points, the medium was removed and the cells were lysed with 5% (w/v) SDS. Thereafter, the fluorescence intensities of GFP or cherry cell homogenates, which corresponded to the appropriate cell number of cancer cells, were measured at an excitation of 485 nm and an emission of 520 nm (GFP), or an excitation of 584 nm and an emission of 612 nm (cherry) using the Fluoroscan Ascent Fl (ThermoFisher Scientific, Schwerte, Germany).

4.3. In Vivo Experiments

About 2x 10^6 human MDA-MB-231^{GFP} and MDA-hyb5 breast cancer cells were subcutaneously injected into the left shoulder of 5 animals from 5–6 weeks old female NODscid mice, respectively. The mice were examined and weighted two times per week. Tumors smaller than 1mm^3 induced by MDA-MB-231^{GFP} cells became detectable between 10 and 18 days. After 32 days following MDA-MB-231^{GFP} cell transplantation the 5 tumor-bearing animals were sacrificed by cervical dislocation following criteria for termination of the experiment. Tumors induced by MDA-hyb5 cells were determined in 4 mice subsequently at later and different time points between 49 days and 161 days. One mouse remained without detectable tumor after 180 days of MDA-hyb5 cell injection.

Primary tumor tissues were isolated, washed in PBS, and weighted. Together with the dissected organs including lung, liver, spleen, kidney, heart, and brain, the tissues were washed in PBS, examined by fluorescence microscopy for the presence and accumulation of metastatic cells, shock-frozen in liquid nitrogen, and stored at -80°C for further analysis. Bone marrow was harvested

by cutting the femur and rinsing the open bone with PBS followed by centrifugation (360g / 7min) of the bone marrow cells.

4.4. Transcript Analysis by PCR

Total RNA was isolated from the tumor tissues and the organs using RNeasy Mini Kit (Qiagen, Hilden, Germany) according to the manufacturer's instructions. One µg of RNA was reverse-transcribed into cDNA, and reactions were performed with corresponding RT-PCR primers:

- mcherry (sense: 5`-TTC ATG TAC GGC TCC AAG GC-3´; antisense: 5`-CTG CTT GAT CTC GCC CTT CA-3´; amplification product 297 bp)
- eGFP (sense: 5`-CTA TAT CAT GGC CGA CAA GCA GA-3´; antisense: 5`-GGA CTG GGT GCT CAG GTA GTG G-3´; amplification product 165 bp)
- CD73 (sense: 5'-CGC AAC AAT GGC ACA ATT AC-3'; antisense: 5'-CTC GAC ACT TGG TGC AAA GA-3'; amplification product 241 bp) [38];
- CD90 (sense: 5'-GGA CTG AGA TCC CAG AAC CA-3'; antisense: 5'-ACG AAG GCT CTG GTC CAC TA-3'; amplification product 124 bp);
- CD105 (sense: 5'-TGT CTC ACT TCA TGC CTC CAG CT-3'; antisense: 5'-AGG CTG TCC ATG TTG AGG CAG T-3'; amplification product 378 bp);
- GAPDH as a control (sense: 5'-ACC ACA GTC CAT GCC ATC AC-3'; antisense: 5'-TCC ACC ACC CTG TTG CTG TA-3'; amplification product 452 bp) [40] (all primers customized by Eurofins, MWG GmbH, Ebersberg, Germany).

Aliquots of 25µl of each RT-PCR product were separated on a 2% agarose gel including the standard GeneRuler 100bp DNA Ladder (Thermo Scientific) and visualized by GelRedTM (Biotium Inc., Hayward, CA, US) staining specifically as described previously [41].

For qPCR, the following primers were used:

- Tumor necrosis factor receptor superfamily member 8 (TNFR SF8, CD30) (sense: 5′-ATC TGT GCC ACA TCA GCC ACC A-3′; antisense: 5′-AAG GTG GTG TCC TTC TCA GCC A-3′; amplification product 110 bp)
- Tumor necrosis factor receptor superfamily member 1B (TNFR SF1B) (sense: 5′-CGT TCT CCA ACA CGA CTT CAT CC-3′; antisense: 5′-ACG TGC AGA CTG CAT CCA TGC T-3′; amplification product 102 bp)
- bone morphogenic protein 1 (BMP1) (sense: 5′-GCC TGT GCT GGT ATG ACT ACG-3′; antisense: 5′-CAT CTG GGT AAT TGG GCG ATT GG-3′; amplification product 243 bp)
- bone morphogenic protein 7 (BMP7) (sense: 5′- ACC AGA GGC AGG CCT GTA AGA-3′; antisense: 5′- CTC ACA GTT AGT AGG CGG CGT AG-3′; amplification product 108 bp)
- transforming growth factor-beta3 (TGF-b3) (sense: 5′-CTA AGC GGA ATG AGC AGA GGA TC-3′; antisense: 5′-TCT CAA CAG CCA CTC ACG CAC A-3′; amplification product 161 bp)
- vascular cell adhesion molecule-1 (VCAM-1) (sense: 5′-GAT TCT GTG CCC ACA GTA AGG C-3′; antisense: 5′-TGG TCA CAG AGC CAC CTT CTT G-3′; amplification product 118 bp)
- Glyceraldehyde 3-phosphate dehydrogenase (GAPDH) (sense: 5′-GTC TCC TCT GAC TTC AAC AGC G-3′; antisense: 5′-ACC ACC CTG TTG CTG TAG CCA A-3′; amplification product 131 bp)
- Ribosomal Protein L13a (RPL13A) (sense: 5′-CTC AAG GTG TTT GAC GGC-3′; antisense: 5′-TAC TTC CAG CCA ACC TCG-3′; amplification product 143 bp)

The QuantiTect SYBR green PCR kit (Qiagen) was used according to the manufacturer's instructions and PCR was performed in quadruplicates using a CFX384 touch real time detection system (Bio-Rad Laboratories GmbH, Feldkirchen, Germany) and analyzed using the BioRad CFX manager software (V.3.1.1517.0823). For normalization of the genes analyzed by qPCR GAPDH and RPL13A were used as housekeeping genes. Melting curves were performed to verify primer quality. High deviation replicates were excluded. The log2 normalized expression values were used for statistical analysis and for generating principle components using GraphPad Prism v9.00.

253

254 *4.5. Microarray-based mRNA expression analysis (Single Color Mode)*

255 The mRNA microarray analyses were performed as extensively described elsewhere [11] with
256 minor modifications. The Microarray utilized in this study represents a refined version of the Whole
257 Human Genome Oligo Microarray 4x44K v2 (Design ID 026652, Agilent Technologies), called
258 '026652QM_RCUG_HomoSapiens' (Design ID 084555) developed by the Research Core Unit
259 Genomics (RCUG) of Hannover Medical School. Microarray design was created at Agilent's eArray
260 portal using a 1x1M design format for mRNA expression as template. All non-control probes of
261 design ID 026652 have been printed five times within a region comprising a total of 181560 Features
262 (170 columns x 1068 rows). Four of such regions were placed within one 1M region giving rise to
263 four microarray fields per slide to be hybridized individually (Customer Specified Feature Layout).
264 Control probes required for proper Feature Extraction software operation were determined and
265 placed automatically by eArray using recommended default settings.

266 Synthesis of Cy3-labeled cRNA was performed with the 'Quick Amp Labeling kit, one color'
267 (#5190-0442, Agilent Technologies) using 500ng of total RNA as input and according to the
268 manufacturer's recommendations, except that reaction volumes were halved. cRNA fragmentation,
269 hybridization and washing steps were carried-out as recommended in the 'One-Color
270 Microarray-Based Gene Expression Analysis Protocol V5.7', except that 3000ng of labelled cRNA
271 were used for hybridization. Slides were scanned on the Agilent Micro Array Scanner G2565CA
272 (pixel resolution 3 μm, bit depth 20). Data extraction was performed with the 'Feature Extraction
273 Software V10.7.3.1' using the extraction protocol file 'GE1_107_Sep09.xml'.

274 The MDA-MB-231^{cherry} cells were investigated together with the cancer hybrid populations
275 MDA-MSC-hyb1, MDA-MSC-hyb3, and MDA-MSC-hyb5. Alterations in transcript levels were
276 compared displaying a more than 2-fold difference in gene expression. Microarray data are stored at
277 the NCBI-GEO database with the accession no. #GSE157199.

278

Results

2.1. Introduction of MDA-MSC-hyb5 (MDA-hyb5) as a new human breast cancer hybrid population

Similar to previous cancer hybrid cell isolations a six day co-culture of 10^6 MDA-MB-231^{cherry} breast cancer cells together with 10^6 primary hUC-MSC030816^{GFP} P4 was performed at a ratio of 50:50 with 4,500 cells/cm^2 in MSC cell growth medium. Following separation of this co-culture for cherry-positive, GFP-positive and double-positive (cherry$^+$ GFP$^+$) cells by two subsequent fluorescence-activated cell sorting (FACS) (1.78 x10^7 total sorted cells yielded 4.24 x10^4 cells after 1. FACS and 3.95 x10^3 cells after 2. FACS) (supplementary Fig. S1) the double positive cells were subjected to single cell cloning. More than 99% of these clones died due to aberrant fusions while a small amount of clones survived and acquired proliferative capactity during a post-hybrid selection process (PHSP). One reason for this striking effect may be the hampered cell division in most hybrid cells by uncoordinated regulatory interactions of the nuclei contents from both fusion partners eventually resulting in cell death [42]. Single cell cloning revealed a proliferating subclone with about 20µm in diameter and predominantly one nucleus after 41d which was termed MDA-MSC-hyb5 (briefly MDA-hyb5) (Fig. 1). Analysis of these MDA-hyb5 cells compared to the two parental MDA-MB-231^{cherry} and hUC-MSC030816^{GFP} populations by RT-PCR demonstrated expression of the mcherry fluorescence gene in MDA-MB-231^{cherry} cells without detectable GFP transcripts, expression of the GFP fluorescence gene in hUC-MSC030816^{GFP} without detectable mcherry transcripts and simultaneous expression of both, the mcherry and the GFP genes in MDA-hyb5 cells. Moreover, MSC typical mRNA transcripts of CD73 and CD105 were detectable in all three cell lines whereas CD90 expression was limited to the hUC-MSC and not detectable in MDA-MB-231 or MSC-hyb5 cells (Fig. 2a). Continuous growth properties of MDA-hyb5 cells were compared to the parental MDA-MB-231 breast cancer cell line and to other related cancer hybrid populations such as MDA-hyb1, MDA-hyb2, MDA-hyb3, and MDA-hyb4 all of which displayed different biological properties [11, 32]. MDA-hyb5 cells demonstrated a similar proliferative capacity like MDA-hyb3 and MDA-hyb4 cells which reached about half of the fastest growing MDA-hyb1

cells and was about 30% less than MDA-hyb2 cells. The rate of MDA-hyb5 cell division increased about 1.8 fold compared to the parental MDA-MB-231^{cherry} breast cancer cells (Fig. 2b). These findings indicated MDA-hyb5 as a new human breast cancer hybrid population with more MDA-MB-231 like properties and an enhanced rate of cell division. Further characterization of MDA-hyb5 cells was performed by short tandem repeat (STR) fragment analysis. In comparison to the STR patterns of the parental MDA-MB-231^{cherry} and hUC-MSC030816^{GFP}, respectively, hyperploidy of MDA-hyb5 cells was detected along with the presentation of 3 and 4 alleles of distinct DNA parts (Fig. 2c).

Because of the different tumor-developing effects reported for other MDA-hybrid populations [11, 32] we were interested in the tumorigenic behavior of MDA-hyb5 cells. Using an in vivo tumor model subcutaneous injection was performed as a control with human MDA-MB-231^{GFP} breast cancer cells into the left shoulder of 5 NODscid mice. After 32 days tumors developed in all the mice (Fig. 3a). A similar subcutaneous injection of MDA-hyb5 cells also developed subcutaneous tumors although at different kinetics. One out of the five mice demonstrated no detectable tumor growth within 180d post injection (Fig. 3b). During the whole experiment all mice displayed a constant body weight without significant changes.

MDA-MB-231-induced tumors were detectable in all injected mice consistent with previous work [11]. This tumor growth became detectable between day 10 and day 18 after injection and was terminated after 32 days by cervical dislocation of the mice according to the animal welfare guidelines. In contrast, MDA-hyb5-induced double fluorescing tumors (mcherry^{+} GFP^{+}) were monitored at subsequent later time points (Table 1).

Table 1. Analysis of tumor development in MDA-MB-231 and MDA-hyb5 tumors

cells (#mouse)	tumor detection [day]	tumor dissection [day]	difference between tumor detection and dissection

			[days]
MDA-MB-231 (#1.2)	10	32	22
MDA-MB-231 (#1.5)	10	32	22
MDA-MB-231 (#1.1)	14	32	18
MDA-MB-231 (#1.4)	14	32	18
MDA-MB-231 (#1.3)	18	32	14
MDA-hyb5 (#2.4)	49	59	10
MDA-hyb5 (#2.5)	70	81	11
MDA-hyb5 (#2.2)	122	131	9
MDA-hyb5 (#2.3)	161	173	12

These data demonstrated that after initial detection subsequent tumor growth by MDA-hyb5 cancer hybrid cells occurred within 10.5 ± 1.3 days, about half of the time compared to the development of the parental MDA-MB-231-induced tumors after 18.8 ± 3.3 days (Fig. 4a). Moreover, the average tumor weight was higher in MDA-hyb5 tumors with 1628 ± 1448 mg as compared to 540 ± 384 mg in MDA-MB-231 tumors although this was not statistically significant (Fig. 4b).

Accordingly, the average time between tumor incidence and dissection revealed a 1.8-fold faster tumor growth induced by MDA-hyb5 cells as compared to the parental MDA-MB-231 cells whereby relative tumor weights remained within a similar range.

Tumor volumes were measured at different time points during tumor development revealing that MDA-MB-231 tumors were 192 to 659 mm (cubed). Similarly, MDA-hyb5 tumors exhibited volumes

between 296 to 711 mm (cubed) at the final point of tumor dissection (Fig. 4c). On the other hand, the incidence of MDA-hyb5-induced tumors occurred at diverse starting time points which were delayed up to 6 months when compared to initial MDA-MB-231-induced tumor detection (Fig. 4c). Following animal examination twice weekly after MDA-hyb5 tumor cell application, initial tumor development became detectable after 49d, 70d, 122d, and 161d, respectively and subsequent tumor growth continued for a short time until termination and tumor dissection (Fig. 4c).

Together, these findings indicated that the MDA-hyb5 cells remained dormant within the mouse tissue in a dormant-like state. Once activated for tumor growth, however, MDA-hyb5 cells developed similar sized tumors 1.8-fold faster compared to MDA-MB-231 cells.

Molecular stimuli and signals for activation of quiescent MDA-hyb5 cells to initiate tumor growth still remain to be elucidated. Accordingly, RNA microarray analysis was performed for comparison with the parental MDA-MB-231 cells and to identify potential expression of dormancy-associated genes. From the 34,126 analysed transcripts 2309 mRNAs were up-regulated and 2913 down-regulated in MDA-hyb5 cells compared to the parental MDA-MB-231 cells (Fig. 5a). Further analyses were performed considering the different tumor behavior of MDA-hyb1 and MDA-hyb3 cells which developed tumors directly after the subcutaneous cancer cell injection in contrast to the initial dormancy phase of MDA-hyb5 cells. In particular, TNF (tumor necrosis factor) ligand- and TNF receptor-associated transcripts were markedly enhanced expressed in MDA-hyb5 as compared to MDA-MB-231 cells in contrast to little if any differences in the MDA-hyb1 versus MDA-MB-231 or the MDA-hyb3 versus MDA-MB-231 expression levels (Fig. 5b). Similar results were obtained for structural genes including entactin (202-fold enhanced in MDA-hyb5) which connects the networks formed by collagens and laminins and transcripts of fibromodulin (228-fold enhanced in MDA-hyb5) participating in the assembly of collagen fibers and restructuring the actin cytoskeleton. Of interest, previous work has demonstrated that laminin-111 in a three-dimensional cell culture system induced quiescence of breast epithelial cells by depletion of nuclear-associated actin [43, 44].

RNA microarrays revealed that gremlin-1 transcripts were 154-fold enhanced expressed in MDA-hyb5 versus MDA-MB-231 whereas little if any expression difference in MDA-hyb1 versus MDA-MB-231 or MDA-hyb3 versus MDA-MB-231 cells were observed (NCBI-GEO database accession no. #GSE157199). Gremlin-1 transcripts are found in various different tumor types and can functionally interfere with the TGF-β (transforming growth factor-beta) signaling pathway by inhibition of the bone morphogenetic proteins BMP2 and BMP4. These findings underscored substantial differences in the tumor behavior of instantly tumor-developing MDA-hyb1 and MDA-hyb3 cells in contrast to a transient initial dormancy phase of MDA-hyb5 cells.

Different genes associated with metastasis and dormancy such as VEGF-A (vascular endothelial growth factor-A) important for vascularization were summarized for primary tumors and distant metastases [45]. Previous work suggested a predominant association of tumor dormancy with cancer stem cells and metastatic cancer cells which promote late recurrences [46]. Moreover, cancer stem cells can disseminate to distal organs early in tumor development [47] suggesting widespread and selective recurrence after dormancy. Thus, BMP signaling selectively relays metastatic relapse of breast cancer cells to the lung [48]. Further dormancy-associated genes include the Wnt/β-catenin signaling cascade [49]. In addition, TGF-β plays an important role during metastasis and dormancy [50, 51]. All of these genes were markedly altered in MDA-hyb5 versus MDA-MB-231. In contrast, only some differences in these gene expressions were detectable in MDA-hyb1 versus MDA-MB-231 or in MDA-hyb3 versus MDA-MB-231 cells (Fig. 5b). Quantitative PCR analysis was performed for these putatively dormancy-related genes and likewise demonstrated modified expression levels (Fig. 5c). A principle components (PC) analysis of the examined genes revealed alterations among the four cell lines. In particular, significant differences were displayed by MDA-hyb5 cells supporting a potentially altered tumorigenic behavior (Fig. 5d).

Whereas MDA-hyb5 cells rapidly developed tumors after an initial dormancy-like phase of up to about 6 months we were interested in the metastatic behavior of these cancer hybrid cells. Cancer cell-expressing GFP although weakly visible in some bands compared to the strong primary tumor

388 was detectable in all tissue aliquots of MDA-MB-231 control cells and MDA-hyb5 cells by RT-PCR
389 (Fig. 6a). Quantification of GFP levels after image J densitometry and normalization by the
390 corresponding GAPDH expression revealed a markedly higher metastatic potential of MDA-hyb5
391 cells as compared to the parental MDA-MB-231 cell line (Fig. 6a, bar diagram). Moreover, thin
392 sections of organ tissues and bone marrow were evaluated by fluorescence microscopy and likewise
393 revealed GFP-carrying cancer cells in all investigated organs (Fig. 6b). Since different
394 MDA-hyb5-induced mice were examined by RT-PCR (mouse #2.5) and by fluorescence microscopy
395 (mouse #2.2) these data suggested appearance of organ metastases in all tumor-carrying MDA-hyb5
396 mice. Indeed, lung tissues from the 4 MDA-hyb5 tumor-bearing mice were analyzed by RT-PCR for
397 mcherry and GFP, respectively, and both transcripts were detectable in the lung tissues (Fig. 6c).

398 In sum, these findings suggested a more rapid tumor development after escape from initial
399 dormancy in MDA-hyb5 cells compared to parental MDA-MB-231 although molecular triggers
400 overcoming this initial quiescence require further investigation.

401 The expression levels of distinct genes associated with tumor dormancy were elevated in MDA-hyb5
402 cells. Moreover, the initiated speedy tumor growth of triggered MDA-hyb5 cells was paralleled by a
403 simultaneously rapid development of organ metastases in all tumor-bearing mice. This aggressive
404 tumor development raised further questions about potential chemotherapeutic approaches.
405 Sensitivities to different concentrations of taxol and epirubicin were compared between parental
406 MDA-MB-231 and MDA-hyb5 cells. While proliferation of MDA-hyb5 control cells was significantly
407 enhanced low concentrations of 100 nM and 300 nM taxol inhibited MDA-hyb5 cell growth more
408 than MDA-MB-231 cells (Fig. 7). However, taxol cytotoxicity displayed a plateau in MDA-hyb5 cells
409 suggesting a constant level of resistance. Higher concentrations of 1 μM epirubicin also
410 demonstrated more sensitivity of MDA-hyb5 cells (Fig. 7).

411 Further chemotherapeutic analyses were performed with explant cultures of dissected MDA-hyb5
412 tumor tissue. The explanted cancer cells in passage 2 and in vitro growing MDA-hyb5 cells were

subjected to different chemotherapeutic treatments. Whereas low drug concentrations of 0.1 nM and 1 nM displayed little if any effects, incubation with epirubicin and taxol at 0.01 μM, 0.1 μM, and 1 μM for 48h up to 72h revealed a concentration-dependent cytotoxicity. Epirubicin treatment reached an about 57% reduction in MDA-hyb5 cells and an about 45% decline in explant tumor cells, respectively, whereby populations formed a plateau (Fig. 8a,b). Moreover, taxol-mediated cytotoxicity revealed about 67% in MDA-hyb5 and about 53% in the corresponding tumor explant cultures. In addition, exposure to 1 μM cyclophosphamide demonstrated about 25% cytotoxicity in MDA-hyb5 cells which was similar in explant tumor cells by about 26% after 72h (Fig. 8a,b).

A more detailed comparison of chemotherapeutic effects with the various drugs revealed little if any difference for epirubicin and carboplatin between MDA-hyb5 cells and the tumor explant culture cells, respectively (supplementary Fig. S2). In contrast, a significantly increased sensitivity to taxol and cyclophosphamide was seen in the tumor explant culture cells which was observed after 48h and 72h, respectively (Fig. 8a,b, supplementary Fig. S2).

Together, these findings suggested a partially enhanced sensitivity of MDA-hyb5 cells to taxol and epirubicin when compared to the parental MDA-MB-231 cells. However, the observed maintenance of a certain basal proliferative level in MDA-hyb5 cells regardless of the applied drug concentration indicated the presence of potentially resistant cancer sub-populations. Moreover, acquisition of partially reduced in vitro sensitivity against epirubicin and taxol in the tumor explant cultures indicated ongoing changes in biological properties during in vivo tumor development.

Discussion

Cell fusion can be part of both physiological and pathophysiological mechansims [52]. Orchestration of signaling to enable cell fusion strongly depends on the cellular microenvironment and may involve alternative kinase pathways e.g. to relay signals for differentiation or apoptosis [53]. Thus,

cell fusion processes can contribute to tissue regeneration such as liver [54]. While cell-cell merger can occur by engulfment of a target cell e.g via cannibalism [55] or entosis-like mechanisms [56] which includes degradation of the target cell genome, fusion-associated MSC hybrid cell formation may be accompanied by a recombination of genomic parts from both parental donors in a nuclear hetero-to-synkaryon transition during subsequent cell division. Since aberrant DNA profiles or aneuploidy can also arise during abnormal cell division like endoreplication, endomitosis or deregulated cytokinesis cancer cell fusion is observed in a variety of different cancer types and derived cancer cell lines [57]. These mechanisms may also promote gene fusions such as RET-fusion which are observed in a variety of colorectal tumors [58, 59]. Although most tumor-generated fusion cells are unable to survive, the remaining hybrid cancer cells can develop a proliferation advantage by overgrowing other cancer cells and eventually representing the majority of a population within a tumor tissue. Moreover, hybrid cancer cells after fusion with MSC can acquire stem cell properties. These effects underscore the significance of tumor fusion mechanisms to alter DNA content and contribute to the severity and worsening of primary tumors and metastatic growth [1, 60, 61].

Cell fusion-mediated aneuploidy causes DNA instabilities and generates aberrant hybrid cells which may be repaired or eliminated by a post-hybrid selection process (PHSP) [33]. A PHSP is associated with chromosomal reduction or reorganization which is required to enable survival of a genetically (meta-)stabilized phenotype after cell-cell merger such as fusion. Therefore, hybrid cell functionalities are determined partially by a multistep program of PHSP [33, 62]. Accordingly, the acquired new properties of MDA-hyb5 cells suggest that besides fusion at least part of this phenotype may represent a consequence of a PHSP during clonal conversion and expansion of the hybrid cancer cells.

Alterations in the DNA profile after fusion causes different properties and tumorigenic behavior in the cancer hybrid cells. While lentiviral transduction processes of the parental MDA-MB-231 and MSC populations themselves already could cause some changes which are unrelated to the fusion process, cancer hybrid cell alterations were identified by comparison to the fluorophore-labeled

parental cell populations rather than to wild-type cells. Fusion-associated changes were different after spontaneous cell merger of MDA-MB-231^{cherry} with several MSC^{GFP}. All breast cancer hybrid populations (MDA-hyb1 to MDA-hyb5) demonstrated significantly increased proliferative capacity when compared to the parental MDA-MB-231^{cherry} cells. Moreover, tumor development and formation of metastases also displayed marked differences. Previous work demonstrated that MDA-hyb1 and MDA-hyb2 cells developed a rapidly enhanced tumor growth and metastases compared to MDA-MB-231 cells [11]. Conversely, MDA-hyb3 and MDA-hyb4 cells also started tumor development after initial subcutaneous injection of the cancer hybrid cells, however, growth of tumors progressed much more slowly as compared to MDA-MB-231 cells. Furthermore, metastasis to distal organs was limited during MDA-hyb3 tumor induction with no detectable metastases in lung and kidney, respectively [32]. In contrast, MDA-hyb5 cells displayed a completely different tumor behavior. Neoplastic tissue by MDA-hyb5 cells became detectable when tumor growth and metastatic development of MDA-MB-231 cells was already terminated. However, when MDA-hyb5 cells initiated tumor growth the progressive development of primary tumors and distal metastases was significantly accelerated as compared to MDA-MB-231 cells. This suggested a rapid tumor neovascularization and enhanced dissemination of MDA-hyb5 cells to enable development of organ metastases nearly twice as fast as MDA-MB-231 cells.

The retarded development of the 4 primary tumors and associated organ metastases induced by MDA-hyb5 cells between 49 days and 161 days post subcutaneous injection indicated dormancy-like states. Dormancy of cancer cells describes a reversible cell cycle arrest similar to a previously suggested G_0' arrest cycle in a differentiation/retrodifferentiation program [63, 64] whereby cells initially enter a transient quiescence. Asymptomatic cell populations can carry dormant cancerous lesions [65] whereby the majority of these lesions never progress to the stage of exponential tumor growth as controlled by hormones and the immune response. Cancer cells may require a temporary G_0' arrest cycle of dormancy for adaptation to altered microenvironmental tissue conditions, coping with chemotherapeutic exposure, or acquisition of new mutations [66]. In particular, disseminated

cancer cells with the potential to metastasize to distant tissues and organs may enter a state of dormancy by moving into a previously suggested transient G_0' arrest cycle to allow adaptation of functionality and metabolism to the new environment.

Although the trigger to awaken MDA-hyb5 cells after at least 161 days for progression of tumor development remains unclear different factors were identified for potential escape from dormancy. A reasonable model for cancer dormancy reflects the bone marrow also as a predominant location for metastases [67]. Previous work suggested that transition of breast cancer cells to dormancy involves accumulation of thrombospondin-1 which can function as an inhibitor of angiogenesis. Vice versa, regained proliferative capacity of the different cancer cell populations is accompanied by neovasculature sprouting and perivascular release of various growth factors [68]. In contrast to the angiogenesis- and neovascularization-associated factor VEGF-A displaying significant changes among the hybrid populations, transcripts of the thrombospondin-1 gene were not markedly altered in MDA-hyb5 cells as compared to MDA-MB-231 cells. However, multiple coordinated signals may be required to maintain cancer cells in dormancy with subsequent triggers to escape the transient G_0' arrest cycle and regain proliferative capacity for tumor development/recurrence. Together, these findings underscore the marked differences of MDA-hyb5 cells as compared to the other hybrids including the initial dormancy-like state of MDA-hyb5 cells which appears unique among the several investigated hybrid breast cancer populations.

Changes in tumor behavior and altered metastatic capacity in cancer hybrid cells is also associated with differences in chemotherapeutic response. The observed unresponsiveness beyond certain concentrations of chemotherapeutic agents indicated a potential resistance within the MDA-hyb5 population. On the other hand, permanent proliferation with self renewal capacity and enhanced resistance to apoptotic stimuli including anti-cancer drugs are also features of cancer progenitor cells, tumor-initiating cells, and cancer stem cells [69, 70]. This is also supported by the elevated resistance acquired by MDA-hyb5 tumor explant cells against taxol and epirubicin suggesting further functional modifications of the cancer hybrid cells during the rapid tumor development and

accounting for instability and an increased heterogeneity. These findings further suggested unstable in vivo phenotypes of MDA-hyb5 cells with continuous alterations which would complicate successful therapeutic regimens.

Conclusions

Characteristics of the breast cancer hybrid cell line MDA-hyb5 demonstrated initial quiescence in vivo. Following release from dormancy the cells developed tumors and metastases much faster than the parental breast cancer cells. Although the trigger for tumor growth in MDA-hyb5 cells requires further elucidation signals for initiated proliferation of these cancer hybrid populations enlarge tumor plasticity and counteract successful interventional strategies. Consequently, the generation and expansion of different cancer hybrid populations in vivo would be associated with bad patient prognoses by frequently ongoing changes and acquisition of new cancer cell functions

Whereas permanent alterations in cancer progenitor cells and cancer stem cells promote therapy resistance and disease progression [71] the appearance of cancer hybrid cells e.g. by MSC/breast cancer cell fusion contributes to elevated cancer cell plasticity. Moreover, the generation of new cancer hybrid cell populations by cell fusion diversifies tumorigenic properties and chemotherapeutic responsiveness which markedly increases tumor heterogeneity. On the other hand, detailed molecular studies using models of initial tumor quiescence enable further insights into tumor dormancy and subsequent tumor initiation also providing a better understanding of mechanisms which trigger tumor relapse and recurrence of metastases.

List of bbreviations

BMP	bone morphogenic protein
CXCR4	C-X-C motif chemokine receptor 4

FACS	fluorescence-activated cell sorting
GFP	green fluorescent protein
hUC	human umbilical cord
MDA-hyb5	MDA-MB-231^{cherry}/MSC030816^{GFP}-hybrid cells (=MDA-MSC-hyb5)
MSC	mesenchymal stroma/stem-like cells
PHSP	post-hybrid selection process
TGF-β	transforming growth factor-beta
TNF	tumor necrosis factor
VCAM-1	vascular cell adhesion molecule-1
VEGF-A	vascular endothelial growth factor-A

Declarations

Ethics approval and consent to participate

Usage of hUC-MSC from human birth-associated tissue was approved by the Ethics Committee of Hannover Medical School, Ethics Committee reference no. #443 on February 26th, 2009 and informed written consent was obtained from each patient.

Animal research using NODscid mice was performed by following the internationally recognized guidelines on animal welfare. The project has been approved by the institutional licensing committee (Niedersächsisches Landesamt für Verbraucherschutz und Lebensmittelsicherheit, Oldenburg, Germany) ref. # 33.19-42502-04-15/1992 on Dec. 17th, 2015.

Consent for publication

Not applicable

Availability of data and materials

Not applicable

Competing interests: The authors declare no conflict of interest.

Funding: This research received no external funding. The APC was supported by the German Research Foundation (DFG) and the Open Access Publication Fund of Hannover Medical School (MHH).

Authors' Contributions: C.M. and T.L. performed the in vitro tests. C.M. and R.H. performed the in vivo experiments. J. v. d.O. isolated and analyzed the exosomes. R.H. designed the study and drafted the manuscript. All authors critically read and approved the final manuscript.

Acknowledgments: The authors are grateful to colleagues from Hannover Medical School: Dr. Matthias Ballmaier (FACS core unit) for fluorescence-activated cell separation; Dr. Oliver Dittrich-Breiholz (Research Core Unit Transcriptomics) for support with the microarray analysis; Dr. Thomas Rothämel (Forensic Medicine) for support with the STR profiling; Dr. Natasha Bogdanova (Radiation Oncology) and Dr. Dhanya Ramachandran (Molecular Gynecology) for support with the qPCR.

References

1. Weiler, J.; Dittmar, T., Cell Fusion in Human Cancer: The Dark Matter Hypothesis. *Cells* **2019,** 8, (2).
2. Ogle, B. M.; Cascalho, M.; Platt, J. L., Biological implications of cell fusion. *Nat Rev Mol Cell Biol* **2005,** 6, (7), 567-75.
3. Duelli, D.; Lazebnik, Y., Cell fusion: a hidden enemy? *Cancer Cell* **2003,** 3, (5), 445-8.
4. Lazova, R.; Laberge, G. S.; Duvall, E.; Spoelstra, N.; Klump, V.; Sznol, M.; Cooper, D.; Spritz, R. A.; Chang, J. T.; Pawelek, J. M., A Melanoma Brain Metastasis with a Donor-Patient Hybrid Genome following Bone Marrow Transplantation: First Evidence for Fusion in Human Cancer. *PLoS One* **2013,** 8, (6), e66731.
5. Noubissi, F. K.; Ogle, B. M., Cancer Cell Fusion: Mechanisms Slowly Unravel. *Int J Mol Sci* **2016,** 17, (9).
6. Shabo, I.; Midtbo, K.; Andersson, H.; Akerlund, E.; Olsson, H.; Wegman, P.; Gunnarsson, C.; Lindstrom, A., Macrophage traits in cancer cells are induced by macrophage-cancer cell fusion and cannot be explained by cellular interaction. *BMC Cancer* **2015,** 15, 922.

7. Clawson, G. A.; Matters, G. L.; Xin, P.; McGovern, C.; Wafula, E.; dePamphilis, C.; Meckley, M.; Wong, J.; Stewart, L.; D'Jamoos, C.; Altman, N.; Imamura Kawasawa, Y.; Du, Z.; Honaas, L.; Abraham, T., "Stealth dissemination" of macrophage-tumor cell fusions cultured from blood of patients with pancreatic ductal adenocarcinoma. *PLoS One* **2017,** 12, (9), e0184451.

8. Wei, H. J.; Nickoloff, J. A.; Chen, W. H.; Liu, H. Y.; Lo, W. C.; Chang, Y. T.; Yang, P. C.; Wu, C. W.; Williams, D. F.; Gelovani, J. G.; Deng, W. P., FOXF1 mediates mesenchymal stem cell fusion-induced reprogramming of lung cancer cells. *Oncotarget* **2014,** 5, (19), 9514-29.

9. Xue, J.; Zhu, Y.; Sun, Z.; Ji, R.; Zhang, X.; Xu, W.; Yuan, X.; Zhang, B.; Yan, Y.; Yin, L.; Xu, H.; Zhang, L.; Zhu, W.; Qian, H., Tumorigenic hybrids between mesenchymal stem cells and gastric cancer cells enhanced cancer proliferation, migration and stemness. *BMC Cancer* **2015,** 15, 793.

10. Noubissi, F. K.; Harkness, T.; Alexander, C. M.; Ogle, B. M., Apoptosis-induced cancer cell fusion: a mechanism of breast cancer metastasis. *FASEB J* **2015,** 29, (9), 4036-45.

11. Melzer, C.; von der Ohe, J.; Hass, R., Enhanced metastatic capacity of breast cancer cells after interaction and hybrid formation with mesenchymal stroma/stem cells (MSC). *Cell Commun Signal* **2018,** 16, (1), 2.

12. Melzer C, v. d. O. J., Hass R., In Vitro Fusion of Normal and Neoplastic Breast Epithelial Cells with Human Mesenchymal Stroma/Stem Cells Partially Involves Tumor Necrosis Factor Receptor Signaling. *Stem Cells* **2018,** 36, (7), 12.

13. Corselli, M.; Chen, C. W.; Sun, B.; Yap, S.; Rubin, J. P.; Peault, B., The tunica adventitia of human arteries and veins as a source of mesenchymal stem cells. *Stem Cells Dev* **2012,** 21, (8), 1299-308.

14. Viswanathan, S.; Shi, Y.; Galipeau, J.; Krampera, M.; Leblanc, K.; Martin, I.; Nolta, J.; Phinney, D. G.; Sensebe, L., Mesenchymal stem versus stromal cells: International Society for Cell & Gene Therapy

(ISCT(R)) Mesenchymal Stromal Cell committee position statement on nomenclature. *Cytotherapy* **2019,** 21, (10), 1019-1024.

15. Hass, R.; Kasper, C.; Bohm, S.; Jacobs, R., Different populations and sources of human mesenchymal stem cells (MSC): A comparison of adult and neonatal tissue-derived MSC. *Cell Commun Signal* **2011,** 9, 12.

16. Caplan, A. I., Mesenchymal Stem Cells: Time to Change the Name! *Stem cells translational medicine* 6, (6), 1445-1451.

17. Boregowda, S. V.; Booker, C. N.; Phinney, D. G., Mesenchymal Stem Cells: The Moniker Fits the Science. *Stem Cells* 36, (1), 7-10.

18. Otte, A.; Bucan, V.; Reimers, K.; Hass, R., Mesenchymal stem cells maintain long-term in vitro stemness during explant culture. *Tissue Eng Part C Methods* **2013,** 19, (12), 937-48.

19. Melzer, C.; Jacobs, R.; Dittmar, T.; Pich, A.; von der Ohe, J.; Yang, Y.; Hass, R., Reversible Growth-Arrest of a Spontaneously-Derived Human MSC-Like Cell Line. *Int J Mol Sci* **2020,** 21, (13).

20. Hu, C.; Li, L., Preconditioning influences mesenchymal stem cell properties in vitro and in vivo. *J Cell Mol Med* **2018,** 22, (3), 1428-1442.

21. Phinney, D. G.; Pittenger, M. F., Concise Review: MSC-Derived Exosomes for Cell-Free Therapy. *Stem Cells* **2017,** 35, (4), 851-858.

22. Hass, R., Role of MSC in the Tumor Microenvironment. *Cancers (Basel)* **2020,** 12, (8).

23. Melzer, C.; Yang, Y.; Hass, R., Interaction of MSC with tumor cells. *Cell Commun Signal* **2016,** 14, (1), 20.

24. Melzer, C.; von der Ohe, J.; Hass, R., Involvement of Actin Cytoskeletal Components in Breast Cancer Cell Fusion with Human Mesenchymal Stroma/Stem-Like Cells. *Int J Mol Sci* **2019,** 20, (4).

634 25. Shilagardi, K.; Li, S.; Luo, F.; Marikar, F.; Duan, R.; Jin, P.; Kim, J. H.; Murnen, K.; Chen, E. H.,
635 Actin-propelled invasive membrane protrusions promote fusogenic protein engagement during
636 cell-cell fusion. *Science* **2013,** 340, (6130), 359-63.
637 26. Pawelek, J. M.; Chakraborty, A. K., The cancer cell--leukocyte fusion theory of metastasis. *Adv Cancer*
638 *Res* **2008,** 101, 397-444.
639 27. Pawelek, J. M.; Chakraborty, A. K., Fusion of tumour cells with bone marrow-derived cells: a unifying
640 explanation for metastasis. *Nat Rev Cancer* **2008,** 8, (5), 377-86.
641 28. Pawelek, J. M., Fusion of bone marrow-derived cells with cancer cells: metastasis as a secondary
642 disease in cancer. *Chin J Cancer* **2014,** 33, (3), 133-9.
643 29. Chitwood, C. A.; Dietzsch, C.; Jacobs, G.; McArdle, T.; Freeman, B. T.; Banga, A.; Noubissi, F. K.; Ogle,
644 B. M., Breast tumor cell hybrids form spontaneously in vivo and contribute to breast tumor metastases.
645 *APL Bioeng* **2018,** 2, (3), 031907.
646 30. Mortensen, K.; Lichtenberg, J.; Thomsen, P. D.; Larsson, L. I., Spontaneous fusion between cancer cells
647 and endothelial cells. *Cell Mol Life Sci* **2004,** 61, (16), 2125-31.
648 31. Weiler, J.; Dittmar, T., Minocycline impairs TNF-alpha-induced cell fusion of M13SV1-Cre cells with
649 MDA-MB-435-pFDR1 cells by suppressing NF-kappaB transcriptional activity and its induction of
650 target-gene expression of fusion-relevant factors. *Cell Commun Signal* **2019,** 17, (1), 71.
651 32. Melzer C, v. d. O. J., Hass R. , In vivo cell fusion between mesenchymal stroma/stem-like cells and
652 breast cancer cells. *Cancers* **2019,** 11, (185).
653 33. Melzer, C.; Ohe, J. V.; Hass, R., Altered Tumor Plasticity after Different Cancer Cell Fusions with MSC.
654 *Int J Mol Sci* **2020,** 21, (21).

655 34. Xu, M. H.; Gao, X.; Luo, D.; Zhou, X. D.; Xiong, W.; Liu, G. X., EMT and acquisition of stem cell-like
656 properties are involved in spontaneous formation of tumorigenic hybrids between lung cancer and
657 bone marrow-derived mesenchymal stem cells. *PLoS One* **2014,** 9, (2), e87893.
658 35. Gauck, D.; Keil, S.; Niggemann, B.; Zanker, K. S.; Dittmar, T., Hybrid clone cells derived from human
659 breast epithelial cells and human breast cancer cells exhibit properties of cancer stem/initiating cells.
660 *BMC Cancer* **2017,** 17, (1), 515.
661 36. Mandel, K.; Yang, Y.; Schambach, A.; Glage, S.; Otte, A.; Hass, R., Mesenchymal stem cells directly
662 interact with breast cancer cells and promote tumor cell growth in vitro and in vivo. *Stem Cells Dev*
663 **2013,** 22, (23), 3114-27.
664 37. Otte, A.; Rauprich, F.; von der Ohe, J.; Yang, Y.; Kommoss, F.; Feuerhake, F.; Hillemanns, P.; Hass, R.,
665 c-Met inhibitors attenuate tumor growth of small cell hypercalcemic ovarian carcinoma (SCCOHT)
666 populations. *Oncotarget* **2015,** 6, (31), 31640-58.
667 38. Yang, Y.; Otte, A.; Hass, R., Human mesenchymal stroma/stem cells exchange membrane proteins and
668 alter functionality during interaction with different tumor cell lines. *Stem Cells Dev* **2015,** 24, (10),
669 1205-22.
670 39. Hass, R.; Bertram, C., Characterization of human breast cancer epithelial cells (HBCEC) derived from
671 long term cultured biopsies. *J Exp Clin Cancer Res* **2009,** 28, 127.
672 40. Otte, A.; Yang, Y.; von der Ohe, J.; Melzer, C.; Hillemanns, P.; Feuerhake, F.; Hass, R., SCCOHT tumors
673 acquire chemoresistance and protection by interacting mesenchymal stroma/stem cells within the
674 tumor microenvironment. *Int J Oncol* **2016,** 49, (6), 2453-2463.

675 41. Melzer, C.; von der Ohe, J.; Hass, R., MSC stimulate ovarian tumor growth during intercellular
676 communication but reduce tumorigenicity after fusion with ovarian cancer cells. *Cell Commun Signal*
677 **2018,** 16, (1), 67.
678 42. Melzer, C.; von der Ohe, J.; Lehnert, H.; Ungefroren, H.; Hass, R., Cancer stem cell niche models and
679 contribution by mesenchymal stroma/stem cells. *Mol Cancer* **2017,** 16, (1), 28.
680 43. Alcaraz, J.; Xu, R.; Mori, H.; Nelson, C. M.; Mroue, R.; Spencer, V. A.; Brownfield, D.; Radisky, D. C.;
681 Bustamante, C.; Bissell, M. J., Laminin and biomimetic extracellular elasticity enhance functional
682 differentiation in mammary epithelia. *EMBO J* **2008,** 27, (21), 2829-38.
683 44. Spencer, V. A.; Costes, S.; Inman, J. L.; Xu, R.; Chen, J.; Hendzel, M. J.; Bissell, M. J., Depletion of
684 nuclear actin is a key mediator of quiescence in epithelial cells. *J Cell Sci* **2011,** 124, (Pt 1), 123-32.
685 45. Neophytou, C. M.; Kyriakou, T. C.; Papageorgis, P., Mechanisms of Metastatic Tumor Dormancy and
686 Implications for Cancer Therapy. *Int J Mol Sci* **2019,** 20, (24).
687 46. Giancotti, F. G., Mechanisms governing metastatic dormancy and reactivation. *Cell* **2013,** 155, (4),
688 750-64.
689 47. Husemann, Y.; Geigl, J. B.; Schubert, F.; Musiani, P.; Meyer, M.; Burghart, E.; Forni, G.; Eils, R.; Fehm,
690 T.; Riethmuller, G.; Klein, C. A., Systemic spread is an early step in breast cancer. *Cancer Cell* **2008,** 13,
691 (1), 58-68.
692 48. Gao, H.; Chakraborty, G.; Lee-Lim, A. P.; Mo, Q.; Decker, M.; Vonica, A.; Shen, R.; Brogi, E.; Brivanlou,
693 A. H.; Giancotti, F. G., The BMP inhibitor Coco reactivates breast cancer cells at lung metastatic sites.
694 *Cell* **2012,** 150, (4), 764-79.

695 49. Ren, D.; Dai, Y.; Yang, Q.; Zhang, X.; Guo, W.; Ye, L.; Huang, S.; Chen, X.; Lai, Y.; Du, H.; Lin, C.; Peng,
696 X.; Song, L., Wnt5a induces and maintains prostate cancer cells dormancy in bone. *J Exp Med* **2019,** 216,
697 (2), 428-449.
698 50. Bragado, P.; Estrada, Y.; Parikh, F.; Krause, S.; Capobianco, C.; Farina, H. G.; Schewe, D. M.;
699 Aguirre-Ghiso, J. A., TGF-beta2 dictates disseminated tumour cell fate in target organs through
700 TGF-beta-RIII and p38alpha/beta signalling. *Nat Cell Biol* **2013,** 15, (11), 1351-61.
701 51. Yumoto, K.; Eber, M. R.; Wang, J.; Cackowski, F. C.; Decker, A. M.; Lee, E.; Nobre, A. R.;
702 Aguirre-Ghiso, J. A.; Jung, Y.; Taichman, R. S., Axl is required for TGF-beta2-induced dormancy of
703 prostate cancer cells in the bone marrow. *Sci Rep* **2016,** 6, 36520.
704 52. Shabo, I.; Svanvik, J.; Lindstrom, A.; Lechertier, T.; Trabulo, S.; Hulit, J.; Sparey, T.; Pawelek, J., Roles of
705 cell fusion, hybridization and polyploid cell formation in cancer metastasis. *World J Clin Oncol* **2020,** 11,
706 (3), 121-135.
707 53. Meinhardt, G.; Roth, J.; Hass, R., Activation of protein kinase C relays distinct signaling pathways in
708 the same cell type: differentiation and caspase-mediated apoptosis. *Cell Death Differ* **2000,** 7, (9),
709 795-803.
710 54. Vassilopoulos, G.; Wang, P. R.; Russell, D. W., Transplanted bone marrow regenerates liver by cell
711 fusion. *Nature* **2003,** 422, (6934), 901-4.
712 55. Bartosh, T. J.; Ullah, M.; Zeitouni, S.; Beaver, J.; Prockop, D. J., Cancer cells enter dormancy after
713 cannibalizing mesenchymal stem/stromal cells (MSCs). *Proc Natl Acad Sci U S A* **2016,** 113, (42),
714 E6447-E6456.
715 56. Sottile, F.; Aulicino, F.; Theka, I.; Cosma, M. P., Mesenchymal stem cells generate distinct functional
716 hybrids in vitro via cell fusion or entosis. *Sci Rep* **2016,** 6, 36863.

57. Melzer, C.; von der Ohe, J.; Hass, R., Concise Review: Crosstalk of Mesenchymal Stroma/Stem-Like Cells with Cancer Cells Provides Therapeutic Potential. *Stem Cells* **2018,** 36, (7), 951-968.

58. Pagani, F.; Randon, G.; Guarini, V.; Raimondi, A.; Prisciandaro, M.; Lobefaro, R.; Di Bartolomeo, M.; Sozzi, G.; de Braud, F.; Gasparini, P.; Pietrantonio, F., The Landscape of Actionable Gene Fusions in Colorectal Cancer. *Int J Mol Sci* **2019,** 20, (21).

59. Pietrantonio, F.; Di Nicolantonio, F.; Schrock, A. B.; Lee, J.; Morano, F.; Fuca, G.; Nikolinakos, P.; Drilon, A.; Hechtman, J. F.; Christiansen, J.; Gowen, K.; Frampton, G. M.; Gasparini, P.; Rossini, D.; Gigliotti, C.; Kim, S. T.; Prisciandaro, M.; Hodgson, J.; Zaniboni, A.; Chiu, V. K.; Milione, M.; Patel, R.; Miller, V.; Bardelli, A.; Novara, L.; Wang, L.; Pupa, S. M.; Sozzi, G.; Ross, J.; Di Bartolomeo, M.; Bertotti, A.; Ali, S.; Trusolino, L.; Falcone, A.; de Braud, F.; Cremolini, C., RET fusions in a small subset of advanced colorectal cancers at risk of being neglected. *Ann Oncol* **2018,** 29, (6), 1394-1401.

60. Gast, C. E.; Silk, A. D.; Zarour, L.; Riegler, L.; Burkhart, J. G.; Gustafson, K. T.; Parappilly, M. S.; Roh-Johnson, M.; Goodman, J. R.; Olson, B.; Schmidt, M.; Swain, J. R.; Davies, P. S.; Shasthri, V.; Iizuka, S.; Flynn, P.; Watson, S.; Korkola, J.; Courtneidge, S. A.; Fischer, J. M.; Jaboin, J.; Billingsley, K. G.; Lopez, C. D.; Burchard, J.; Gray, J.; Coussens, L. M.; Sheppard, B. C.; Wong, M. H., Cell fusion potentiates tumor heterogeneity and reveals circulating hybrid cells that correlate with stage and survival. *Sci Adv* **2018,** 4, (9), eaat7828.

61. Jiang, E.; Yan, T.; Xu, Z.; Shang, Z., Tumor Microenvironment and Cell Fusion. *Biomed Res Int* **2019,** 2019, 5013592.

62. Hass, R.; von der Ohe, J.; Ungefroren, H., Impact of the Tumor Microenvironment on Tumor Heterogeneity and Consequences for Cancer Cell Plasticity and Stemness. *Cancers (Basel)* **2020,** 12, (12).

738 63. Hass, R., Retrodifferentiation--an alternative biological pathway in human leukemia cells. *Eur J Cell*
739 *Biol* **1992,** 58, (1), 1-11.
740 64. Hass, R., Retrodifferentiation and cell death. *Crit Rev Oncog* **1994,** 5, (4), 359-71.
741 65. Folkman, J.; Kalluri, R., Cancer without disease. *Nature* **2004,** 427, (6977), 787.
742 66. Recasens, A.; Munoz, L., Targeting Cancer Cell Dormancy. *Trends Pharmacol Sci* **2019,** 40, (2), 128-141.
743 67. Widner, D. B.; Park, S. H.; Eber, M. R.; Shiozawa, Y., Interactions Between Disseminated Tumor Cells
744 and Bone Marrow Stromal Cells Regulate Tumor Dormancy. *Curr Osteoporos Rep* **2018,** 16, (5), 596-602.
745 68. Ghajar, C. M.; Peinado, H.; Mori, H.; Matei, I. R.; Evason, K. J.; Brazier, H.; Almeida, D.; Koller, A.;
746 Hajjar, K. A.; Stainier, D. Y.; Chen, E. I.; Lyden, D.; Bissell, M. J., The perivascular niche regulates breast
747 tumour dormancy. *Nat Cell Biol* **2013,** 15, (7), 807-17.
748 69. Ye, X.; Tam, W. L.; Shibue, T.; Kaygusuz, Y.; Reinhardt, F.; Ng Eaton, E.; Weinberg, R. A., Distinct EMT
749 programs control normal mammary stem cells and tumour-initiating cells. *Nature* **2015,** 525, (7568),
750 256-60.
751 70. Kreso, A.; Dick, J. E., Evolution of the cancer stem cell model. *Cell Stem Cell* **2014,** 14, (3), 275-91.
752 71. Meacham, C. E.; Morrison, S. J., Tumour heterogeneity and cancer cell plasticity. *Nature* **2013,** 501,
753 (7467), 328-37.
754 72. Tomayko, M. M.; Reynolds, C. P., Determination of subcutaneous tumor size in athymic (nude) mice.
755 *Cancer Chemother Pharmacol* **1989,** 24, (3), 148-54.
756 73. Yang, Y.; Melzer, C.; Bucan, V.; von der Ohe, J.; Otte, A.; Hass, R., Conditioned umbilical cord tissue
757 provides a natural three-dimensional storage compartment as in vitro stem cell niche for human
758 mesenchymal stroma/stem cells. *Stem Cell Res Ther* **2016,** 7, 28.
759

760 **Figure legends**

761 **Figure 1.**

762 The morphology and a preparation sequence are demonstrated for the generation and isolation of
763 MDA-MSC-hyb5 (MDA-hyb5) cells. The upper panel represents mcherry fluorescence, the middle
764 panel GFP fluorescence, and the lower panel the corresponding phase contrast micrographs. Bars
765 represent 200μm.

766

767 **Figure 2.**

768 (**a**) Gene expression in steady state cultured MDA-hyb5 cells was compared to the parental
769 MDA-MB-231^{cherry} and hUC-MSC030816^{GFP} populations by RT-PCR whereby GAPDH transcripts
770 served as an equal loading control. (**b**) Measurement of proliferative capacity was performed in
771 steady state growing cell lines of parental MDA-MB-231^{cherry} breast cancer cells and several fused
772 hybrid populations by fluoroscan assay. Data were normalized to control cells at 24h indicating
773 relative fluorescence which correlates to relative proliferative capacity as previously described [38].
774 Data represent the mean ± s.d. of 8 replicates, respectively. (c) Short tandem repeat (STR) fragment
775 analysis of MDA-hyb5 cells was performed in comparison to the parental MDA-MB-231^{cherry} and
776 hUC-MSC030816^{GFP} cells.

777

778 **Figure 3.**

779 (**a**) MDA-MB-231-induced tumors (after 32 d) and (**b**) tumors induced by MDA-hyb5 cells. Tumor
780 tissues after subcutaneous injection of 2x 10^6 MDA-MB-231^{GFP} or MDA-hyb5 cells, respectively, were
781 dissected from NODscid mice at the indicated time points and weighted.

782

783 **Figure 4.**

784 (**a**) The average time between the earliest detection of tumors and following dissection after growth
785 of the tumors was calculated and compared between parental MDA-MB-231 cells (n=5) and fusion

786 hybrid MDA-hyb5 cells (n=4). Significance (p) was calculated by unpaired student's t-test. (**b**) The
787 average tumor weight of MDA-MB-231- and MDA-hyb5-induced tumors was calculated by the
788 mean ± s.d., respectively. Differences were not significant. (**c**) After tumor cell injection of
789 MDA-MB-231 (mouse #1.1 to #1.5) and MDA-hyb5 (mouse #2.2 to #2.5) into the NODscid mice the
790 tumors became first detectable at the indicated time points. Continuous tumor growth and detection
791 of appropriate sizes were measured using a digital caliper. Progressive tumor volumes to the
792 corresponding time points were calculated with the longitudinal diameter (length) and the
793 transverse diameter (width) in the modified ellipsoidal formula: volume=$\pi/6$ x width x $(\text{length})^2$ as
794 previously reported [37, 72].
795
796 **Figure 5.**
797 (**a**) RNA microarray analysis of 34,126 transcripts was performed in MDA-hyb5 cells as compared to
798 the parental MDA-MB-231 cells. Changes in transcript levels below 2-fold were considered below
799 cut-off. (**b**) Analysis of the RNA microarray data was performed with a focus on the expression of
800 dormancy-associated genes (tumor necrosis factor receptor superfamily member 8 (TNFR SF8);
801 tumor necrosis factor receptor superfamily member 1B (TNFR SF1B); bone morphogenic protein1
802 (BMP1); bone morphogenic protein7 (BMP7); transforming growth factor-beta3 (TGF-beta3);
803 vascular endothelial growth factor-A (VEGF-A)). Differences in fold changes are indicated for the
804 relationship of gene expression in MDA-MSC-hyb5 (hyb5), MDA-MSC-hyb3 (hyb3), and
805 MDA-MSC-hyb1 (hyb1) cells versus the parental MDA-MB-231 (MDA) cells, respectively. (**c**) Gene
806 expression levels were normalized to GAPDH and RPL13A by qPCR. Data represent the mean $\pm$
807 SEM of the corrected expression levels (n=4) and significance (p) was calculated by the Dunnett's
808 multiple comparison ANOVA test (ns=not significant). (**d**) A scattered plot of principle components
809 (PC) was generated by GraphPad Prism v9.00 and demonstrated the differences between the cell
810 lines according to the genes analyzed.
811
812 **Figure 6.**

(**a**) Following dissection of MDA-MB-231^{GFP} control cells- and MDA-hyb5 (mouse #2.5) cells-induced primary tumors and distal organ metastases including lung, liver, spleen, kidney, heart, and brain, preparation of bone marrow was performed from femoral content and RNA aliquots were subjected to RT-PCR for GFP. GAPDH transcripts served as an equal loading control. Normalization of GFP expression levels by the corresponding GAPDH ratios was performed by densitometry scanning using the image J software. The resulting quantitatively comparable GFP expression levels in the different organs are demonstrated as a logarithmic bar diagram in the lower panel. (**b**) Distal organs and bone marrow from mouse #2.2 were dissected after euthanization and evaluated by fluorescence microscopy whereby appropriate fluorescence should indicate formation of distant metastases. Bars represent 100µm. (**c**) Aliquots of lung metastases from all 4 MDA-hyb5-induced mouse tumors including a corresponding no template control (NTC) were subjected to RT-PCR for mcherry and GFP detection. GAPDH transcripts served as an equal loading control.

Figure 7.

MDA-MB-231 and MDA-hyb5 cells were treated with the indicated concentrations of taxol and epirubicin for 24 h to 72 h, respectively. Thereafter, the cells were lyzed and measured by fluoroscan assay. The data were normalized to the 24h control cells. The relative data represent the mean ± s.d. of 3 independent experiments with 3 replicates each. Significance (p) was calculated by unpaired student's t-test.

Figure 8.

(**a**) MDA-hyb5 cells and (**b**) explant cells from cultured MDA-hyb5-induced tumor #2.5 after dissection were exposed to different chemotherapeutic agents for up to 72h. Untreated control cells (white bars on the left) were followed by constantly increasing drug concentrations between 0.1 nM to 1 µM (colored bars). After treatment with the corresponding drug at the indicated concentration and incubation time the cells were lyzed and measured by fluoroscan assay. Data were normalized

and relative fluorescence correlated to relative proliferative capacity as previously described [73]. Data represent the mean ± s.d. of 3 independent experiments with 3 replicates each.

Supplementary Materials:

Suppl. Figure S1: Purification of double positive cells from the co-culture (left dot blot histogram) demonstrated accumulation of mcherry$^+$ cells, GFP$^+$ cells and a double positive population (mcherry$^+$ GFP$^+$) after the second sort (right dot blot histogram).

Suppl. Figure S2: Relative 72h chemosensitivities for the different drug cytotxicities were compared between MDA-hyb5 cells and explant cells from cultured mouse tumor #2.5 after dissection. Significance (p) was calculated by unpaired student's t-test.

Figures

Fig. 1

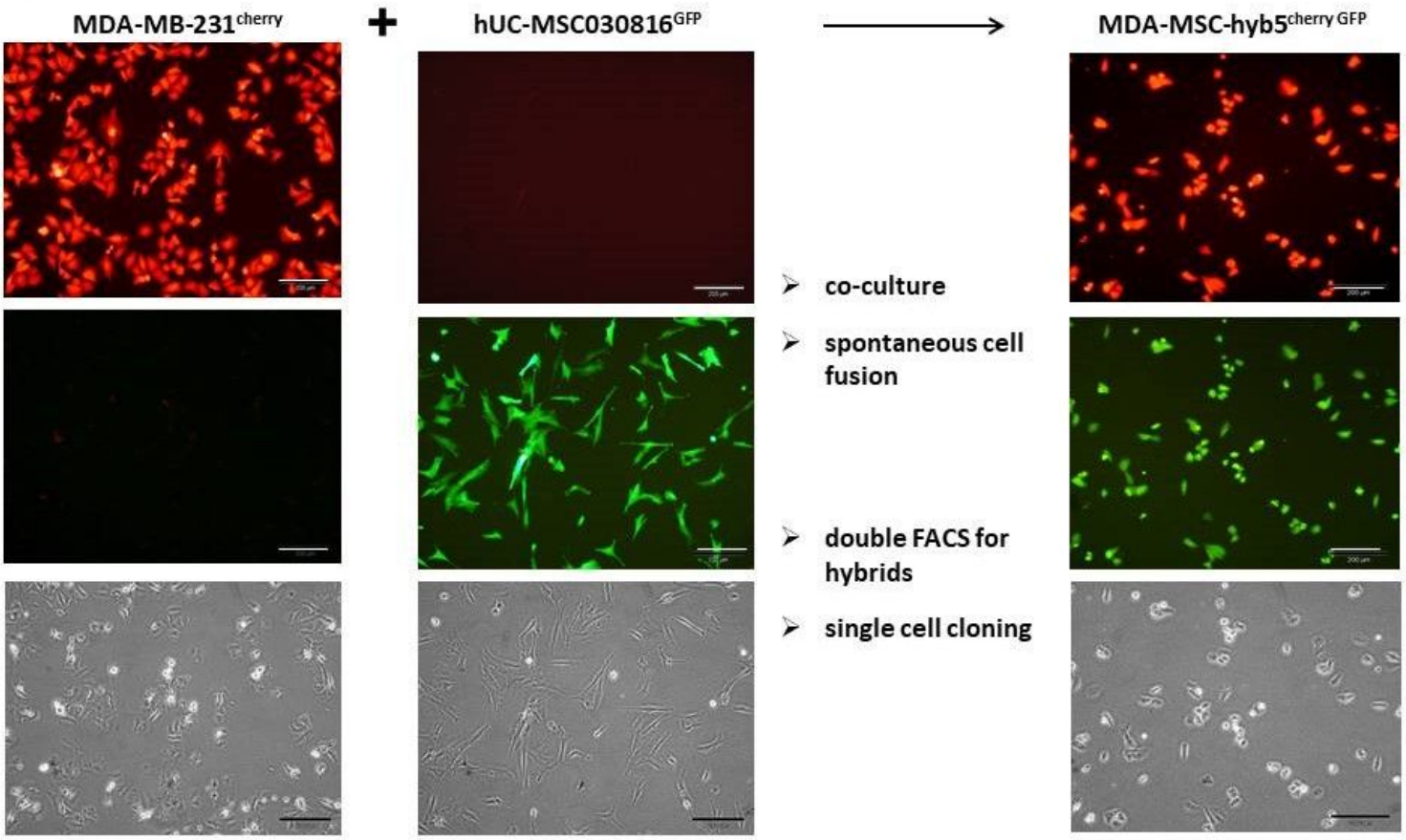

Figure 1

The morphology and a preparation sequence are demonstrated for the generation and isolation of MDA-MSC-hyb5 (MDA-hyb5) cells. The upper panel represents mcherry fluorescence, the middle panel GFP fluorescence, and the lower panel the corresponding phase contrast micrographs. Bars represent 200µm.

Fig. 2

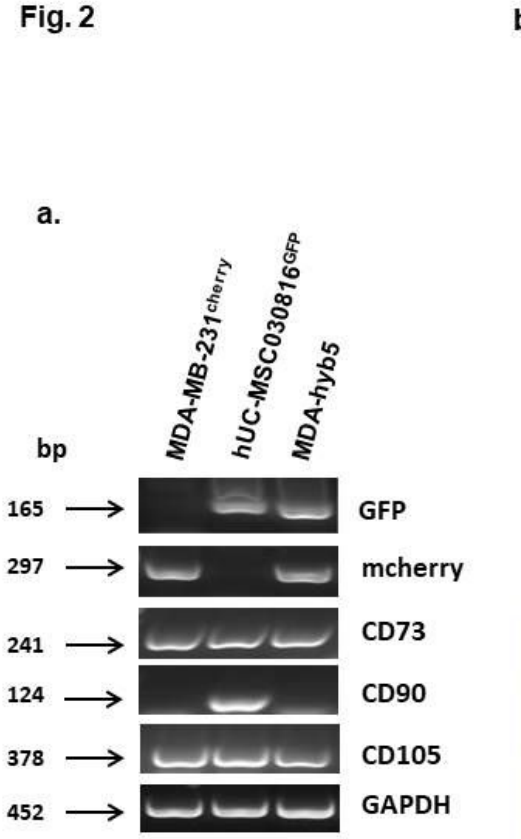

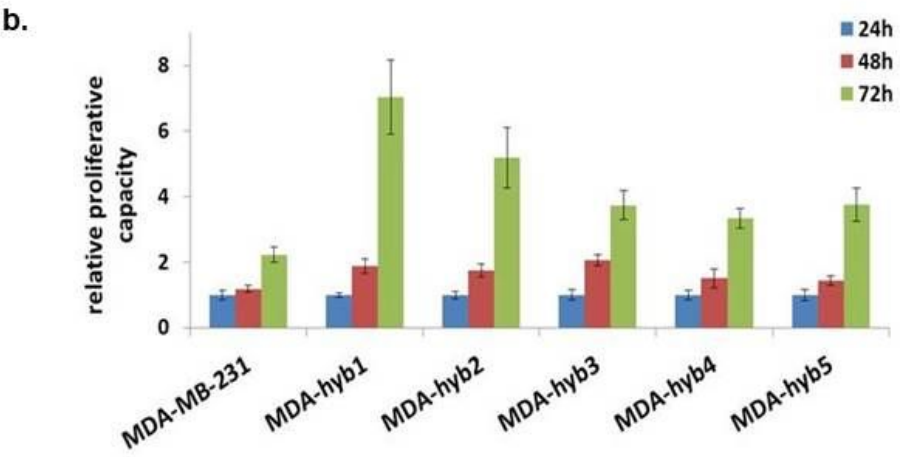

c.

	MDA-MB-231cherry		MSC030816GFP P2		MDA-hyb5 P2			
STR fragment	allel 1	allel 2	allel 1	allel 2	allel 1	allel 2	allel 3	allel 4
Amelogenin	X-chrom.		X-chrom.	Y-chrom.	X-chrom.			
D10S1248	16		14		16			
D12S391	17	18	17	18.3	17	18	18.3	
D16S539	12		12	14	12			
D18S51	11		16		11	16		
D19S433	12	14	12	14	12	14		
D1S1656	15	17	11	16	11	15	16	17
D21S11	33.2		28	31.2	33.2			
D22S1045	16	17	15		16	17		
D2S1338	20	21	18	25	20	21	25	
D2S441	14	15	11	14	14	15		
D3S1358	16		14	16	16			
D8S1179	13		12	13	13			
FGA	22	23	20	21	22	23		
SE33	15		19	23.2	15	23.2		
TH01	7	9.3	6	9.3	7	9.3		
VWA	15	18	16		15	16	18	

Figure 2

(a) Gene expression in steady state cultured MDA-hyb5 cells was compared to the parental MDA-MB-231cherry and hUC-MSC030816GFP populations by RT-PCR whereby GAPDH transcripts served as an equal loading control. (b) Measurement of proliferative capacity was performed in steady state growing cell lines of parental MDA-MB-231cherry breast cancer cells and several fused hybrid populations by fluoroscan assay. Data were normalized to control cells at 24h indicating relative fluorescence which correlates to relative proliferative capacity as previously described [38]. Data represent the mean ± s.d. of 8 replicates, respectively. (c) Short tandem repeat (STR) fragment analysis of MDA-hyb5 cells was performed in comparison to the parental MDA-MB-231cherry and hUC-MSC030816GFP cells.

Fig. 3

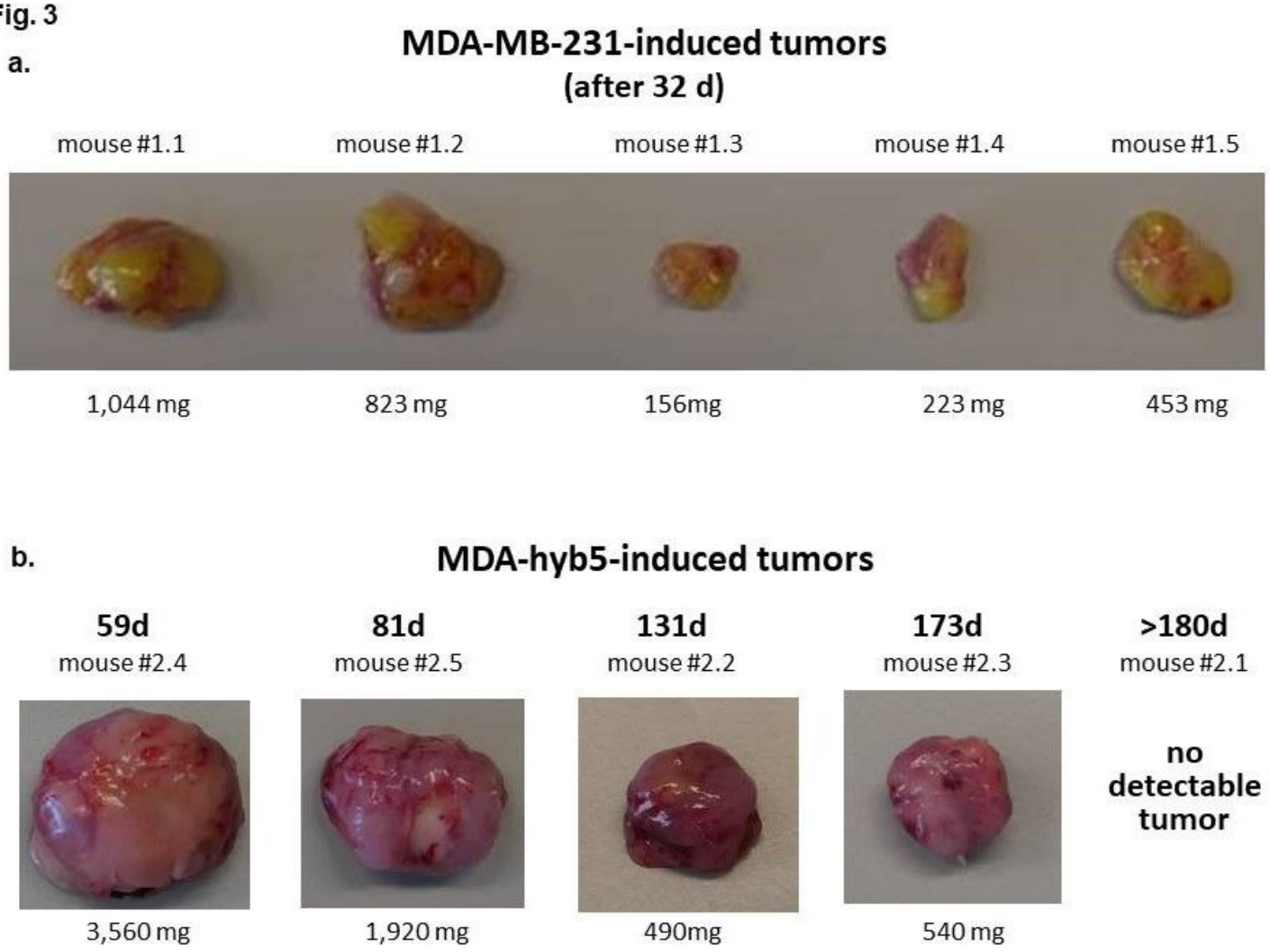

Figure 3

(a) MDA-MB-231-induced tumors (after 32 d) and (b) tumors induced by MDA-hyb5 cells. Tumor tissues after subcutaneous injection of 2x 106 MDA-MB-231GFP or MDA-hyb5 cells, respectively, were dissected from NODscid mice at the indicated time points and weighted.

Fig. 4

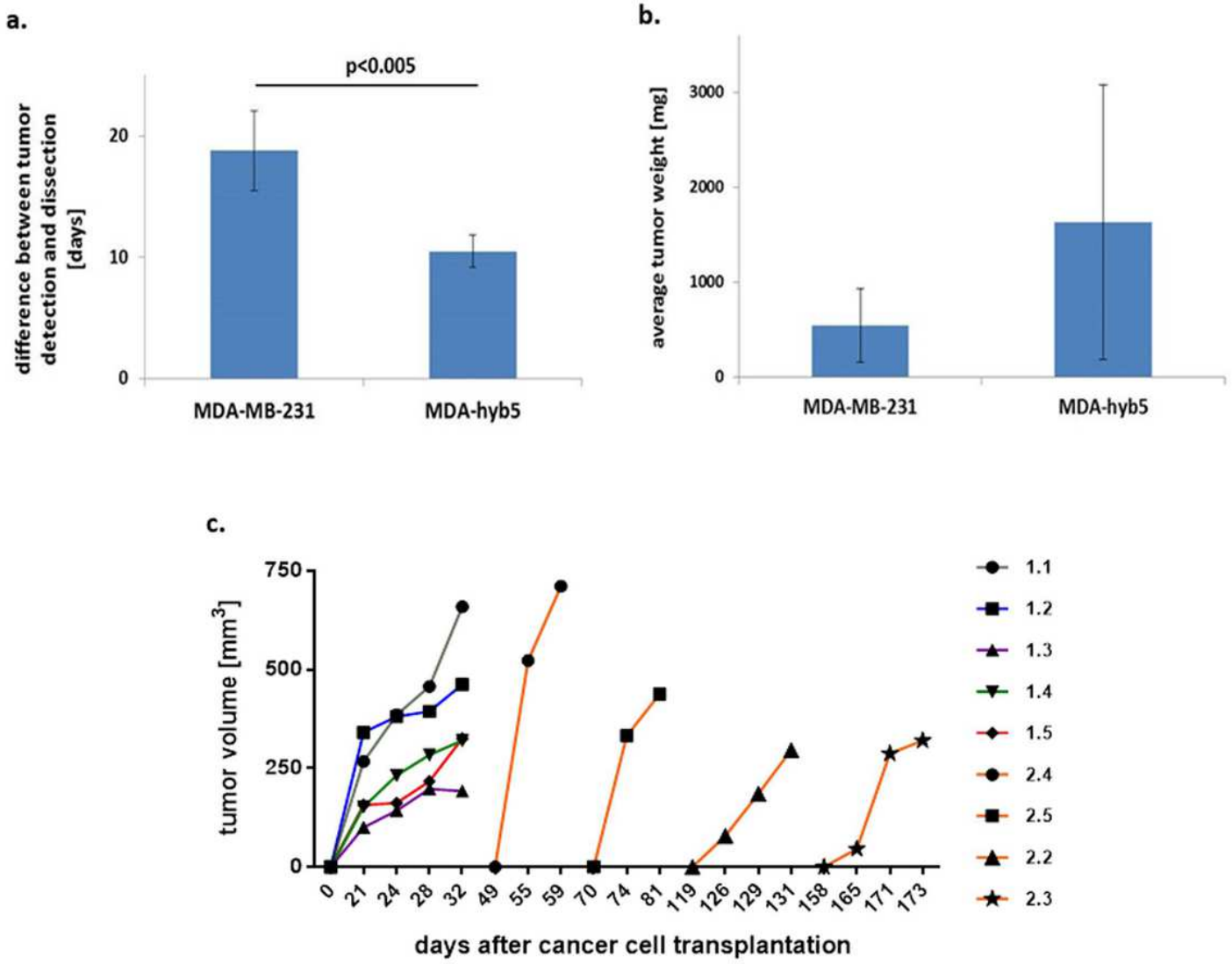

Figure 4

(a) The average time between the earliest detection of tumors and following dissection after growth of the tumors was calculated and compared between parental MDA-MB-231 cells (n=5) and fusion hybrid MDA-hyb5 cells (n=4). Significance (p) was calculated by unpaired student's t-test. (b) The average tumor weight of MDA-MB-231- and MDA-hyb5-induced tumors was calculated by the mean ± s.d., respectively. Differences were not significant. (c) After tumor cell injection of MDA-MB-231 (mouse #1.1 to #1.5) and MDA-hyb5 (mouse #2.2 to #2.5) into the NODscid mice the tumors became first detectable at the indicated time points. Continuous tumor growth and detection of appropriate sizes were measured using a digital caliper. Progressive tumor volumes to the corresponding time points were calculated with the longitudinal diameter (length) and the transverse diameter (width) in the modified ellipsoidal formula: volume=π/6 x width x (length)2 as previously reported [37, 72].

Fig. 5

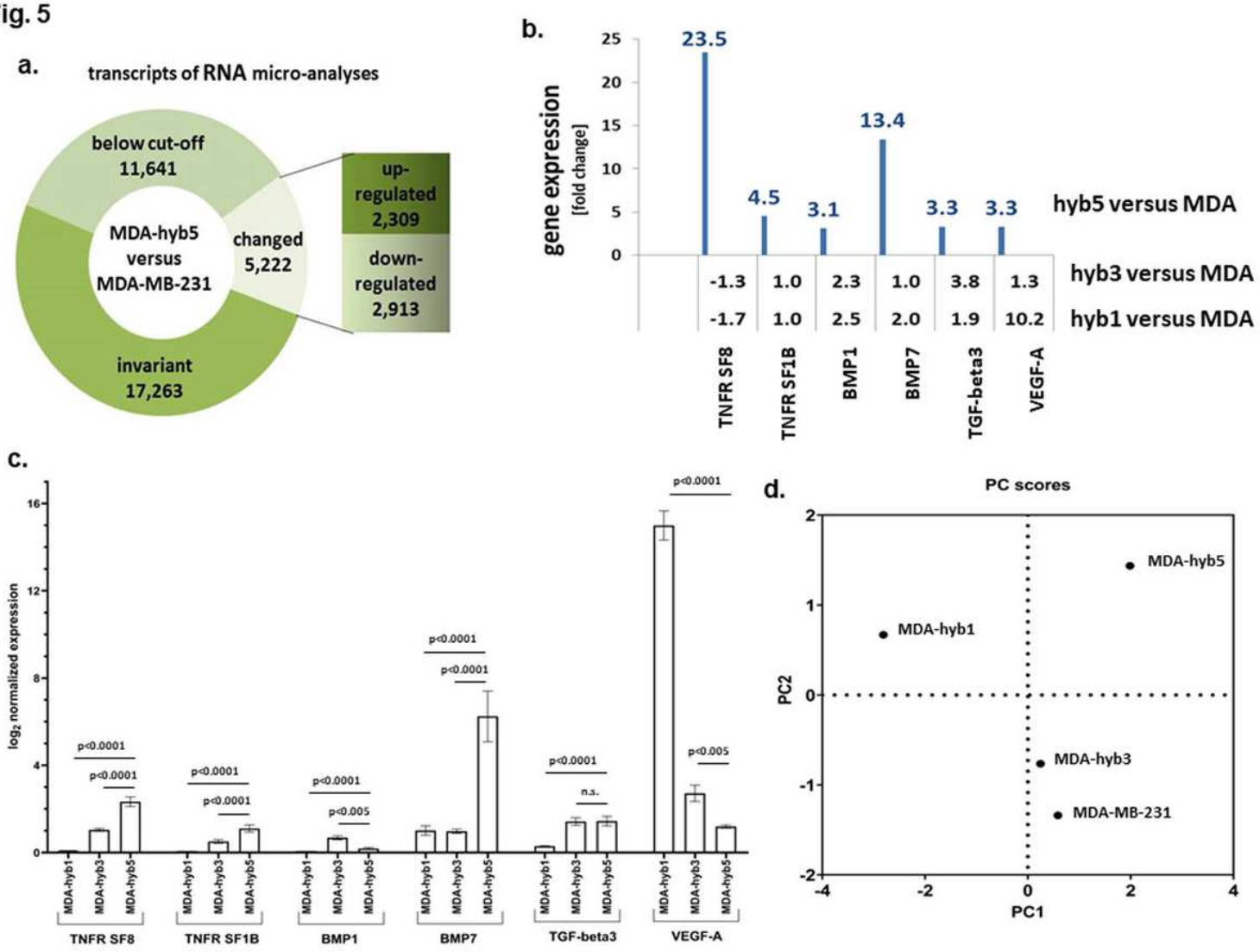

Figure 5

a) RNA microarray analysis of 34,126 transcripts was performed in MDA-hyb5 cells as compared to the parental MDA-MB-231 cells. Changes in transcript levels below 2-fold were considered below cut-off. (b) Analysis of the RNA microarray data was performed with a focus on the expression of dormancy-associated genes (tumor necrosis factor receptor superfamily member 8 (TNFR SF8); tumor necrosis factor receptor superfamily member 1B (TNFR SF1B); bone morphogenic protein1 (BMP1); bone morphogenic protein7 (BMP7); transforming growth factor-beta3 (TGF-beta3); vascular endothelial growth factor-A (VEGF-A)). Differences in fold changes are indicated for the relationship of gene expression in MDA-MSC-hyb5 (hyb5), MDA-MSC-hyb3 (hyb3), and MDA-MSC-hyb1 (hyb1) cells versus the parental MDA-MB-231 (MDA) cells, respectively. (c) Gene expression levels were normalized to GAPDH and RPL13A by qPCR. Data represent the mean + SEM of the corrected expression levels (n=4) and significance (p) was calculated by the Dunnett's multiple comparison ANOVA test (ns=not significant). (d) A scattered plot of principle components (PC) was generated by GraphPad Prism v9.00 and demonstrated the differences between the cell lines according to the genes analyzed.

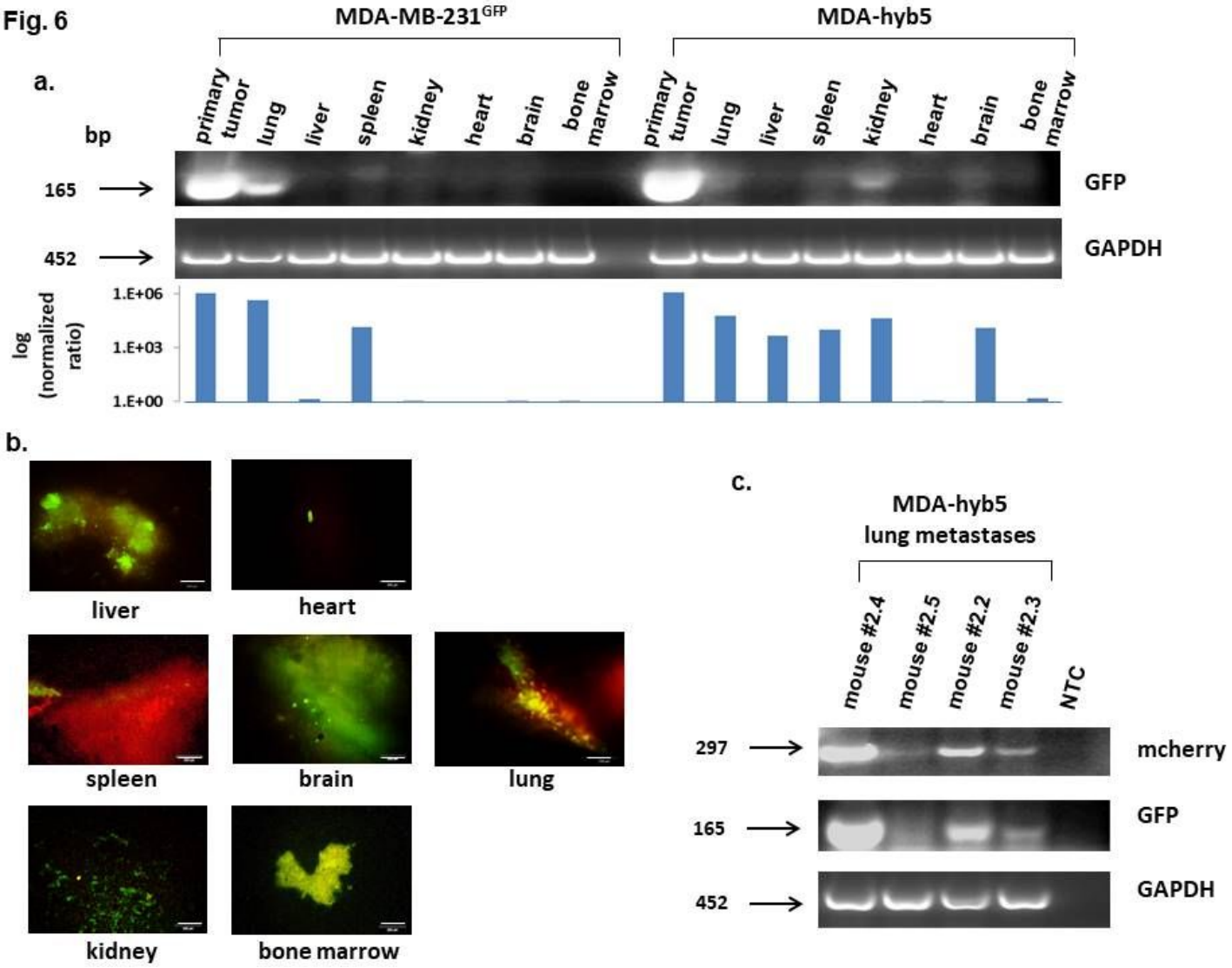

Figure 6

a) Following dissection of MDA-MB-231GFP control cells- and MDA-hyb5 (mouse #2.5) cells- induced primary tumors and distal organ metastases including lung, liver, spleen, kidney, heart, and brain, preparation of bone marrow was performed from femoral content and RNA aliquots were subjected to RT-PCR for GFP. GAPDH transcripts served as an equal loading control. Normalization of GFP expression levels by the corresponding GAPDH ratios was performed by densitometry scanning using the image J software. The resulting quantitatively comparable GFP expression levels in the different organs are demonstrated as a logarithmic bar diagram in the lower panel. (b) Distal organs and bone marrow from mouse #2.2 were dissected after euthanization and evaluated by fluorescence microscopy whereby appropriate fluorescence should indicate formation of distant metastases. Bars represent 100µm. (c) Aliquots of lung metastases from all 4 MDA-hyb5-induced mouse tumors including a corresponding no template control (NTC) were subjected to RT-PCR for mcherry and GFP detection. GAPDH transcripts served as an equal loading control.

Fig. 7

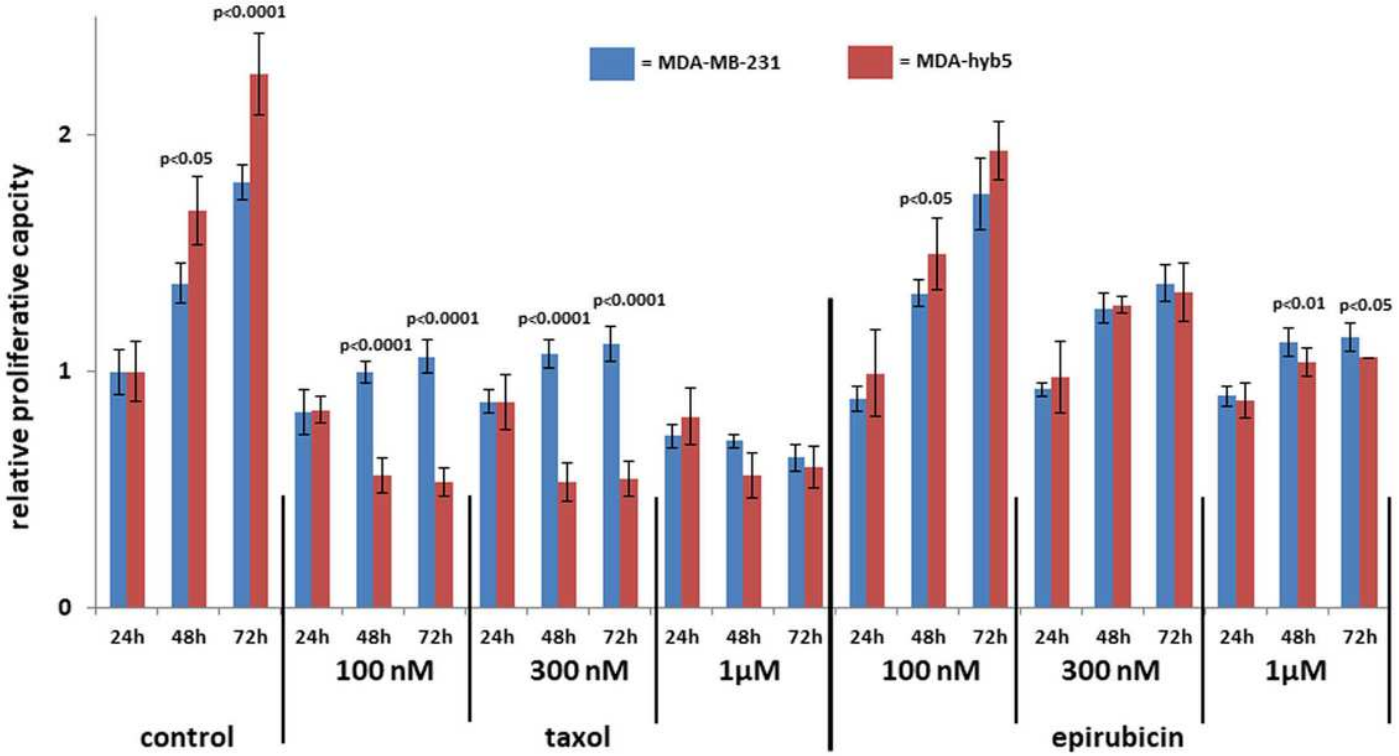

Figure 7

MDA-MB-231 and MDA-hyb5 cells were treated with the indicated concentrations of taxol and epirubicin for 24 h to 72 h, respectively. Thereafter, the cells were lyzed and measured by fluoroscan assay. The data were normalized to the 24h control cells. The relative data represent the mean ± s.d. of 3 independent experiments with 3 replicates each. Significance (p) was calculated by unpaired student's t-test.

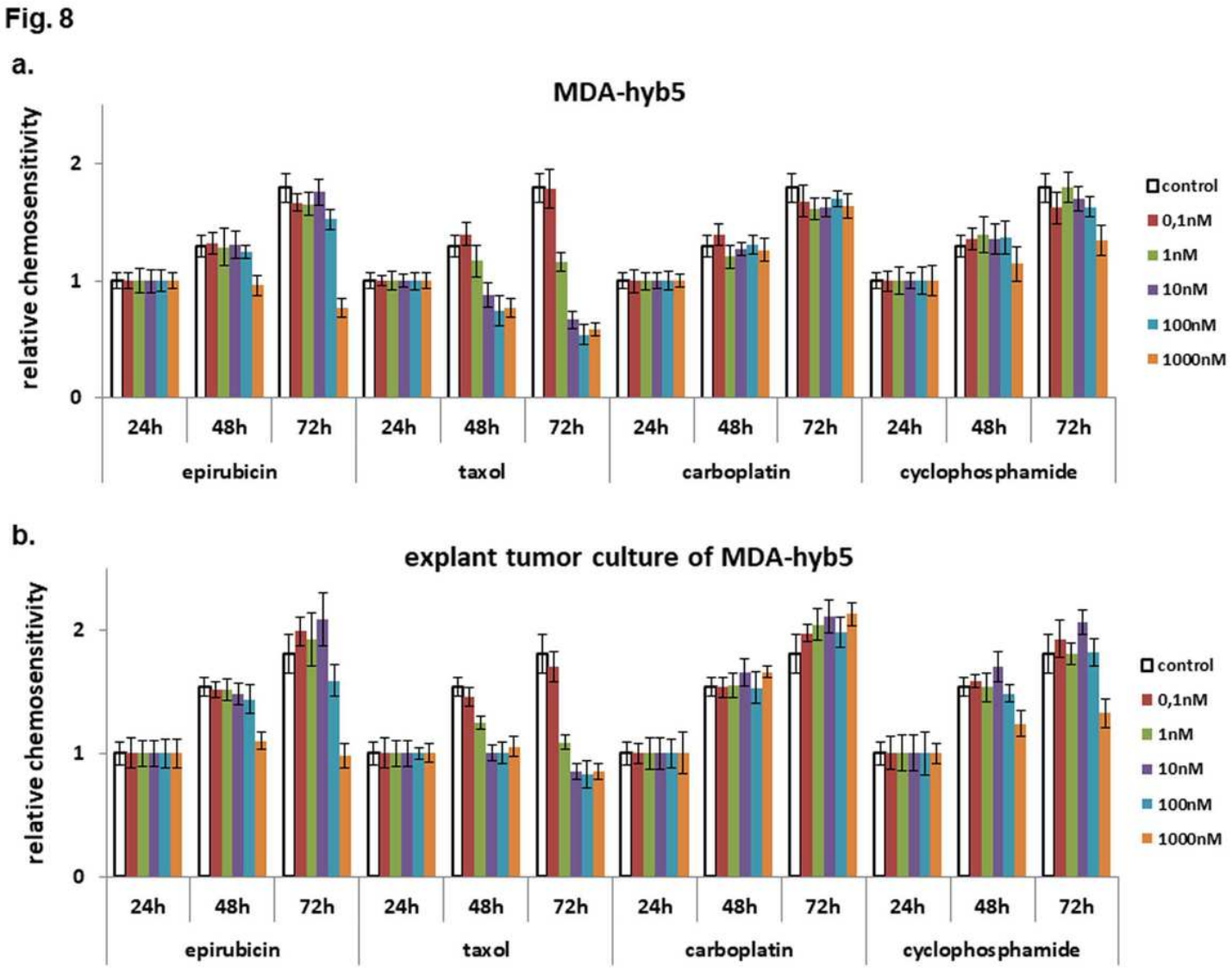

Figure 8

a) MDA-hyb5 cells and (b) explant cells from cultured MDA-hyb5-induced tumor #2.5 after dissection were exposed to different chemotherapeutic agents for up to 72h. Untreated control cells (white bars on the left) were followed by constantly increasing drug concentrations between 0.1 nM to 1 µM (colored bars). After treatment with the corresponding drug at the indicated concentration and incubation time the cells were lyzed and measured by fluoroscan assay. Data were normalized and relative fluorescence correlated to relative proliferative capacity as previously described [73]. Data represent the mean ± s.d. of 3 independent experiments with 3 replicates each.

Supplementary Files

This is a list of supplementary files associated with this preprint. Click to download.

- suppl.Fig.S1CCSFACSsorthyb5.jpg

- suppl.Fig.S2CCSChemotest.tif